

62272 DV

AFATL-TR-71-149

A METHOD FOR ELIMINATING
THE
MAGNUS INSTABILITY OF A FINNED MISSILE

GUN RANGE OPERATIONS BRANCH
GUNS AND ROCKETS DIVISION

TECHNICAL REPORT AFATL-TR-71-149

NOVEMBER 1971

DDC
RECEIVED
MAY 15 1972
RECEIVED
C

Reproduced by
NATIONAL TECHNICAL
INFORMATION SERVICE
Springfield, VA 22151

Approved for public release; distribution
unlimited.

AIR FORCE ARMAMENT LABORATORY

AIR FORCE SYSTEMS COMMAND • UNITED STATES AIR FORCE

EGLIN AIR FORCE BASE, FLORIDA

UNCLASSIFIED

Security Classification

DOCUMENT CONTROL DATA - R & D

(Security classification of title, body of abstract and indexing annotation must be entered when the overall report is classified)

1. ORIGINATING ACTIVITY (Corporate author) Guns and Rockets Division Air Force Armament Laboratory Eglin Air Force Base, Florida 32542		2a. REPORT SECURITY CLASSIFICATION Unclassified	
3. REPORT TITLE A METHOD FOR ELIMINATING THE MAGNUS INSTABILITY OF A FINNED MISSILE		2b. GROUP	
4. DESCRIPTIVE NOTES (Type of report and inclusive dates)			
5. AUTHOR(S) (First name, middle initial, last name) Edward S. Sears			
6. REPORT DATE November 1971	7a. TOTAL NO. OF PAGES 66	7b. NO. OF REFS 8	
8a. CONTRACT OR GRANT NO	9a. ORIGINATOR'S REPORT NUMBER(S) AFATL-TR-71-149		
b. PROJECT NO	9b. OTHER REPORT NO(S) (Any other numbers that may be assigned this report)		
c.			
d.			
10. DISTRIBUTION STATEMENT Approved for public release, distribution unlimited.			
11. SUPPLEMENTARY NOTES Available in DDC		12. SPONSORING MILITARY ACTIVITY Air Force Armament Laboratory Air Force Systems Command Eglin Air Force Base, Florida 32542	
13. ABSTRACT Subsonic one-degree-of-freedom and three-degrees-of-freedom wind tunnel tests were performed to determine whether N-vanes attached to a spinning, statically stable missile would eliminate the Magnus instabilities which can occur at high spin rates. The clean configuration missile that was tested had a large precession limit cycle of about 35 degrees amplitude. With N-vanes at + 15 degrees, it was possible to eliminate the precession limit cycle. With the N-vanes at -15 degrees, the precession limit cycle was eliminated, and a nutation limit cycle of 25 degrees was created. The motion of the missile with and without N-vanes was photographed with a high speed camera. The angular data obtained were fit using the WOBBLE computer program to obtain the coefficients of pitching moment, pitch damping moment, and Magnus moment. Smoke flow pictures were taken of each configuration to determine how the flow over the model was affected by the N-vanes. The aerodynamic coefficients obtained were found to be nonlinear with angle of attack. These coefficients verified the observed changes in the dynamic stability of the missile that occurred with the addition of the N-vanes.			

UNCLASSIFIED

Security Classification

14 KEY WORDS	LINK A		LINK B		LINK C	
	ROLE	WT	ROLE	WT	ROLE	WT
Magnus Instability						
Finned Missile						
Wind Tunnel Tests						
Linear Aeroballistic Theory						

**A Method for Eliminating
the
Magnus Instability of a Finned Missile**

Edward S. Sears

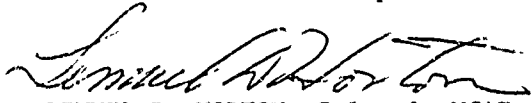
Approved for public release; distribution
unlimited.

FOREWORD

This technical report is based on a thesis submitted by the author to the Graduate School of the University of Notre Dame in partial fulfillment of the requirements for the degree of Master of Science in Aerospace Engineering. No Air Force funds were involved in the research leading to this report; however, the subject matter is significant to the design and development of missile weapon systems.

Drs. J. D. Nicolaidis and C. W. Ingram provided guidance in the preparation of this report, R. S. Eikenberry assisted in reducing and fitting the data, and D. W. Lando assisted in performing the experimental program and analyzing the data.

This technical report has been reviewed and is approved.



LEMUEL D. HORTON, Colonel, USAF
Chief, Guns and Rockets Division

ABSTRACT

Subsonic one-degree-of-freedom and three-degrees-of-freedom wind tunnel tests were performed to determine whether N-vanes attached to a spinning, statically stable missile would eliminate the Magnus instabilities which can occur at high spin rates. The clean configuration missile that was tested had a large precession limit cycle of about 35 degrees amplitude. With N-vanes at + 15 degrees, it was possible to eliminate the precession limit cycle. With the N-vanes at -15 degrees, the precession limit cycle was eliminated, and a nutation limit cycle of 25 degrees was created. The motion of the missile with and without N-vanes was photographed with a high speed camera. The angular data obtained were fit using the WOBBLE computer program to obtain the coefficients of pitching moment, pitch damping moment, and Magnus moment. Smoke flow pictures were taken of each configuration to determine how the flow over the model was affected by the N-vanes. The aerodynamic coefficients obtained were found to be nonlinear with angle of attack. These coefficients verified the observed changes in the dynamic stability of the missile that occurred with the addition of the N-vanes.

Approved for public release; distribution unlimited.

TABLE OF CONTENTS

Section		Page
I	Introduction	1
II	Linear Aeroballistic Theory	4
III	Experimental Technique	12
	1. Inertia Measurement	12
	2. Wind Tunnel Testing Procedure	12
	3. 1-D Wind Tunnel Testing Procedure	12
	4. 1-D Data Reduction Procedure	12
	5. 3-D Wind Tunnel Testing Procedure	16
	6. 3-D Data Reduction Procedure	16
	7. Flow Visualization Technique	17
IV	Results	22
V	Analysis of Data	23
	1. Results for Clean Configuration	50
	2. Results for N-Vane 1 Configuration	50
	3. Results for N-Vane 2 Configuration	50
	4. Results of Flow Visualization Tests	50
	5. Results in Nonlinear Data Reduction	51
VI	Conclusions and Recommendations	54
	References	55

LIST OF FIGURES

Number	Title	Page
1	Low Drag Finned Configuration	2
2	Configuration Tested	3
3	Aeroballistic Axis System	4
4	Force and Moment System	8
5	Example of 3-D Angular Motion (N-Vanes 1)	9
6	Nutation Limit Cycle (N-Vane 1) Configuration	10
7	Data from N-Vane 1 Configuration (Run 1)	11
8	3-D Support System	13
9	Wind Tunnel Test Models	14
10	1-D Test Set-Up	15
11	1-D Data Reduction Procedure	18
12	3-D Wind Tunnel Set-Up	19
13	3-D Reference Point System	20
14	Reduction of Tunnel Motion to Angular Data	21
15	$C_{M\alpha}$ for Clean Configuration from 1-D Tests	24
16	$(C_{M\alpha} + C_{M\dot{\alpha}})$ for Clean Configuration from 1-D Tests	25
17(a)	Pitching Moment Coefficient for Clean Configuration	26
(b)	Pitching Moment Coefficient for N-Vane 1 Configuration	27
(c)	Pitching Moment Coefficient for N-Vane 2 Configuration	28
18(a)	Pitch Damping Moment Coefficient for Clean Configuration	29
(b)	Pitch Damping Moment Coefficient for N-Vane 1 Configuration	30
(c)	Pitch Damping Moment Coefficient for N-Vane 2 Configuration	31
19(a)	Magnus Moment Coefficient for Clean Configuration	32
(b)	Magnus Moment Coefficient for N-Vane 1 Configuration	33
(c)	Magnus Moment Coefficient for N-Vane 2 Configuration	34
20(a)	Nutation Frequency for Clean Configuration from 3-D Test	35
(b)	Nutation Frequency for N-Vane 1 Configuration from 3-D Test	36
(c)	Nutation Frequency for N-Vane 2 Configuration	37
21(a)	Precession Frequency for Clean Configuration from 3-D Test	38
(b)	Precession Frequency for N-Vane 1 Configuration from 3-D Test	39
(c)	Precession Frequency for N-Vane 2 Configuration	40
22(a)	Nutation Dynamic Damping Factor for Clean Configuration from 3-D Test	41
(b)	Nutation Dynamic Damping Factor for N-Vane 1 Configuration from 3-D Test	42
(c)	Nutation Dynamic Damping Factor for N-Vane 2 Configuration from 3-D Test	43
23(a)	Precession Dynamic Damping Factor for Clean Configuration from 3-D Test	44

LIST OF FIGURES (Concluded)

Number	Title	Page
23(b)	Precession Dynamic Damping Factor for N-Vane 1 Configuration from 3-D Test	45
(c)	Precession Dynamic Damping Factor for N-Vane 2 Configuration	46
24	Summary of Aerodynamic Coefficients	47
25	Dynamic Damping Factors for Limit Cycle Motions	48
26	Smoke Flow over Clean Configuration	52
27	Smoke Flow over N-Vane Configurations at Steady Spin Rate	53

LIST OF SYMBOLS

C_M	Pitching moment coefficient
	$C_M = \frac{M}{Qs d}$
$C_{M\alpha}$	Pitching moment stability coefficient (rad^{-1})
	$C_{M\alpha} = \frac{\partial C_M}{\partial \alpha} = \frac{M \alpha}{\alpha Qs d}$
C_{Mq}	Damping moment stability coefficient (rad^{-1})
	$C_{Mq} = \frac{\partial C_M}{\partial \frac{qd}{2V}} = \frac{M q}{\frac{qd}{2V} Qs d}$
$C_{M\dot{\alpha}}$	Lag moment stability coefficient (rad^{-1})
	$C_{M\dot{\alpha}} = \frac{\partial C_M}{\partial \frac{\dot{\alpha} d}{2V}} = \frac{M \dot{\alpha}}{\frac{\dot{\alpha} d}{2V} Qs d}$
$C_{Mp\beta}$	Magnus moment stability coefficient (rad^{-2})
	$C_{Mp\beta} = \frac{\partial^2 C_N}{\partial \alpha \partial \frac{pd}{2V}} = \frac{N p \alpha^2}{\frac{pd}{2V} \alpha Qs d} = \frac{M p \beta}{\frac{pd}{2V} \beta Qs d}$
d	Reference length - missile diameter (ft)
I	Transverse moment of inertia ($\text{slug}\cdot\text{ft}^2$)
I_x	Axial moment of inertia ($\text{slug}\cdot\text{ft}^2$)
K_N	Amplitude of nutation mode (degrees)
K_P	Amplitude of precession mode (degrees)
K_R	Amplitude of yaw of repose arm (degrees)
K_T	Amplitude of trim arm (degrees)
P	Roll rate (rad/sec)
p, q, r	Angular velocity components (rad/sec)

LIST OF SYMBOLS (Concluded)

L,M,N	Aerodynamic moments in aeroballistic axis system
\vec{q}	Complex pitching velocity (rad/sec)
	$\vec{q} = q + ir$
Q	Dynamic pressure - $1/2 \rho V^2$ (lb/ft ²)
R	Distance from missile center of gravity to reference point (in.)
s	Gyroscopic stability factor
SF	Scale factor
S	Reference area = $\frac{\pi d^2}{4}$ (ft ²)
t	Time (sec)
u,v,w	Transverse velocity components (ft/sec)
x,y,z	Space fixed axes
X,Y,Z	Aeroballistic axes
V	Total velocity (ft/sec)
α	Angle of attack (degrees or radians)
$\vec{\alpha}$	Complex angle of attack (degrees or radians)
	$\vec{\alpha} = \beta + i\alpha$
β	Angle of sideslip (degrees or radians)
$\lambda_{N,P}$	Nutation and precession dynamic damping factors of linear aeroballistic theory (sec ⁻¹)
ρ	Air density (slugs/ft ³)
$\omega_{N,P}$	Nutation and precession frequencies (rad/sec)
γ	Dynamic weight factor
$ \alpha_M $	Mean angle of attack = $\sqrt{K_N^2 + K_P^2}$ (deg)

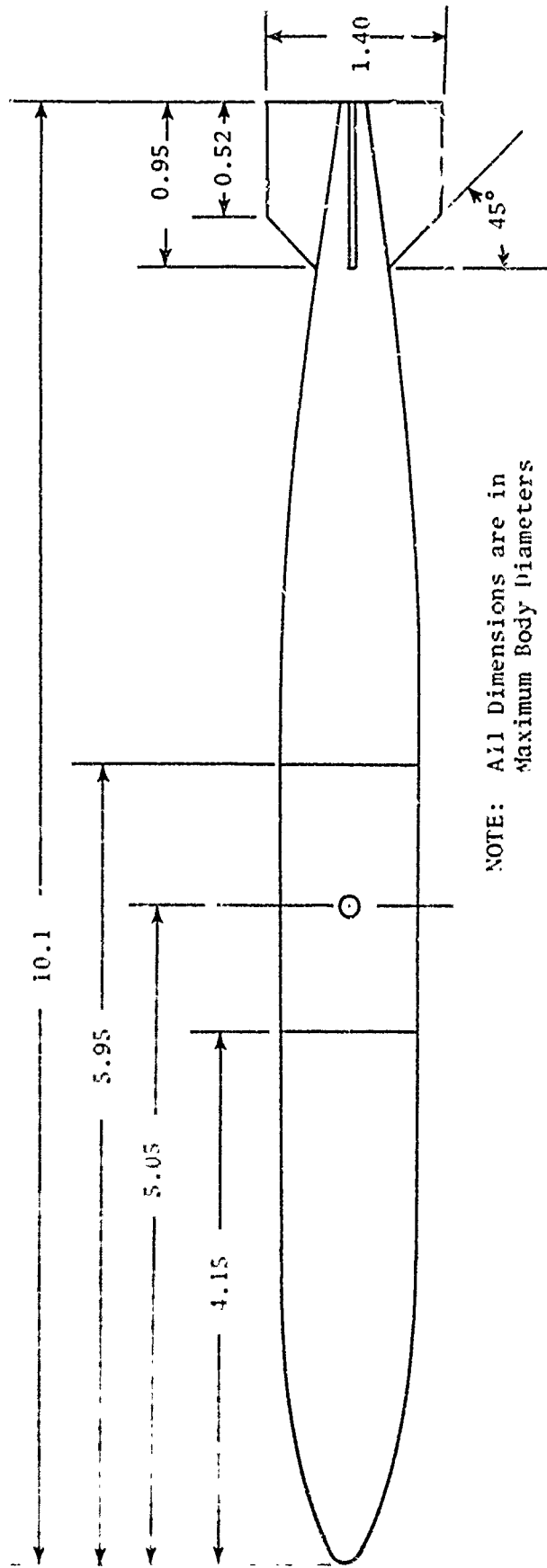
SECTION I

INTRODUCTION

A symmetric-finned missile with static stability does not require spin for dynamic stability (Reference 1). However, manufacturing tolerances are usually sufficient to cause undesirable dispersion when the spin rate is zero; therefore, as explained in Reference 2, most finned missiles are intentionally designed to spin. The spin rate required to reduce dispersion due to asymmetries is usually not large, on the order of a few radians per second. Unfortunately, the nutation frequency of most finned missiles is of the same order of magnitude.

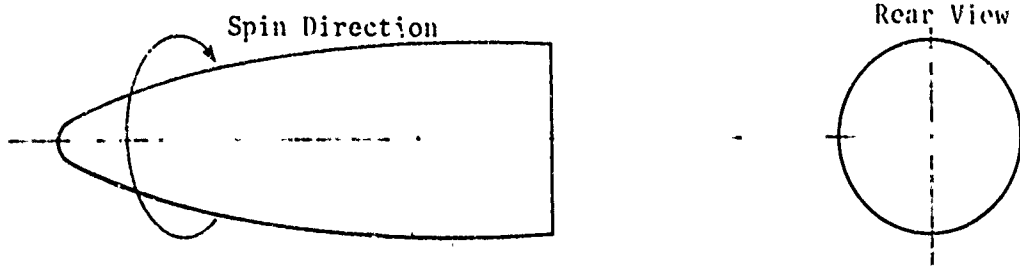
A finned missile is usually designed to spin up to some spin rate above the nutation frequency in order to avoid the resonance instability described in Reference 2. This phenomenon can occur when the spin rate is near the nutation frequency. A spin rate of five times the nutation frequency is usually considered adequate to avoid resonance instability, assuming the missile rolls through the critical region quickly. However, at the higher spin rates, a Magnus instability can occur (Reference 3).

The purpose of the work presented in this report was to determine if these Magnus instabilities could be eliminated by the addition of small very-low-aspect-ratio vanes, N-vanes, to the missile as suggested in References 2 and 3. A finned missile (Figure 1) that was known to have a Magnus instability was selected and after various appendages were added, the changes that the appendage caused in the missile angular motion were observed. After numerous tests, an N-vane configuration was found that significantly altered the missile motion. The angular motions of the successful N-vane configurations, as well as of the basic or clean configuration (Figure 2), were then fit to the aeroballistic theory from Reference 4, and the aerodynamic coefficients were obtained.

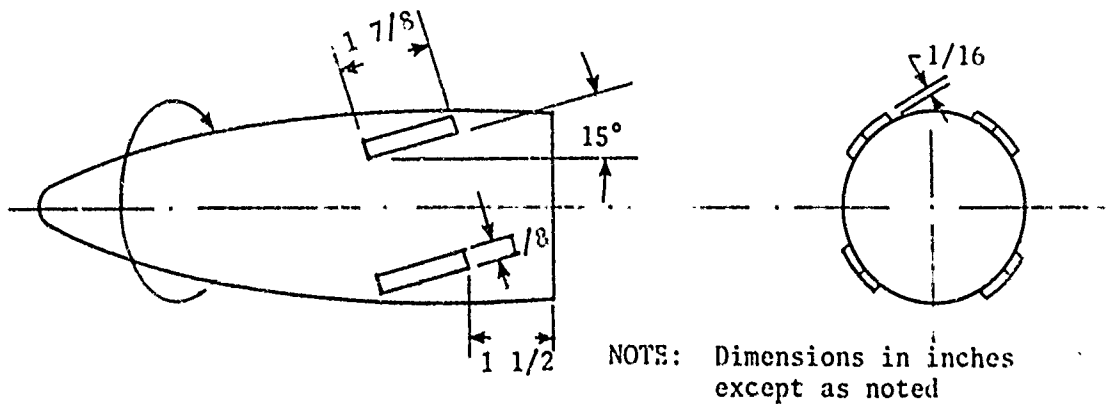


NOTE: All Dimensions are in Maximum Body Diameters

Figure 1. Low Drag Finned Configuration

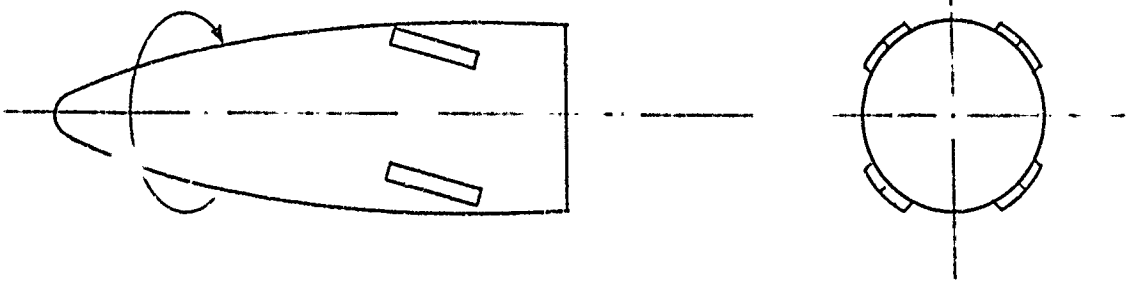


(a) Clean Configuration



NOTE: Dimensions in inches except as noted

(b) N-vane 1 Configuration (-)



(c) N-vane 2 Configuration (+)

Figure 2. Configuration Tested

SECTION II

LINEAR AEROBALLISTIC THEORY

The angular equations of motion for a symmetric missile with a constrained center of gravity are

$$\begin{aligned} L &= I_X \dot{p} \\ M &= I_q \dot{q} + p I_X r \\ N &= I_r \dot{r} - p I_X \dot{q} \end{aligned} \quad (1)$$

Where the forces and moments are described in an aeroballistic axis system as shown in Figure 3.

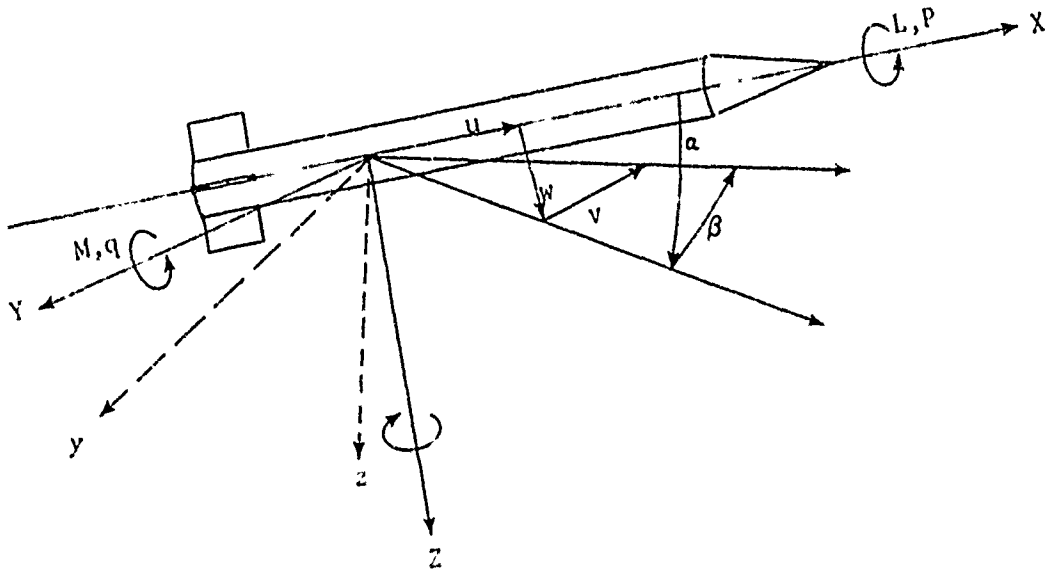


Figure 3. Aeroballistic Axis System

For a constant roll rate, $L = 0$ and the aerodynamic moments are.

$$M = M_{\alpha} \alpha + M_q q + M_{\dot{\alpha}} \dot{\alpha} + M_{p\beta} p \beta \quad (2)$$

$$N = N_{\beta}\beta + N_r r + N_{\dot{\beta}}\dot{\beta} + N_{p\alpha} p\alpha \quad (3)$$

For a missile with trigonal, or greater, rotational symmetry and mirror symmetry about the longitudinal axis, the following relations exist among the aerodynamic stability derivatives

$$N_{\beta} = -M_{\alpha} \quad N_{\dot{\beta}} = -M_{\dot{\alpha}} \quad (4)$$

$$N_r = M_q \quad N_{p\alpha} = M_{p\beta} \quad (5)$$

Making use of the relations $q = \dot{\alpha}$ and $r = -\dot{\beta}$ for small angles, the moment equations may be written as follows

$$M_{\alpha}\ddot{\alpha} + M_q\dot{\alpha} + M_{\dot{\alpha}}\dot{\alpha} + M_{p\beta}p\beta = i\ddot{\alpha} - pI_x\beta \quad (6)$$

$$-M_{\alpha}\ddot{\beta} - M_q\dot{\beta} - M_{\dot{\alpha}}\dot{\beta} + M_{p\beta}p\alpha = -i\ddot{\beta} - pI_x\dot{\alpha} \quad (7)$$

Multiplying Equation (6) by i and Equation (7) by -1 and then adding the results give

$$M_{\alpha}\ddot{\vec{\alpha}} + M_q\dot{\vec{\alpha}} + M_{\dot{\alpha}}\dot{\vec{\alpha}} + iM_{p\beta}p\vec{\alpha} = i\ddot{\vec{\alpha}} - ipI_x\dot{\vec{\alpha}} \quad (8)$$

Where $\vec{\alpha} = \beta + i\alpha$.

Rearranging Equation (8) gives

$$\ddot{\vec{\alpha}} - \left[\frac{M_q + M_{\dot{\alpha}}}{I} + ipI_x/I \right] \dot{\vec{\alpha}} - \left[\frac{M_{\alpha}}{I} + \frac{ipM_{p\beta}}{I} \right] \vec{\alpha} = 0 \quad (9)$$

The solution to Equation (9) is

$$\ddot{\alpha} = K_N e^{(\lambda_N + i\omega_N)t} + K_P e^{(\lambda_P + i\omega_P)t} + K_T e^{ipt} + K_R \quad (10)$$

Where

$$\lambda_{N,P} = \frac{QSd^2}{2I} \left[\frac{(C_{Mq} + C_{M\dot{\alpha}})}{2I} (1 \pm \tau) \pm C_{Mp\beta} \frac{\tau}{I_x} \right] \quad (11)$$

$$\omega_{N,P} = \frac{PI_x}{2I} \left(1 \pm \frac{1}{\tau} \right) \quad (12)$$

$$\tau = \frac{1}{\sqrt{1 - \frac{1}{S}}} \quad (\text{Dynamic weight factor}) \quad (13)$$

$$s = \frac{(I_x p)^2}{4IC_{M\dot{\alpha}}QSd} \quad (\text{Gyroscopic stability factor}) \quad (14)$$

For a statically stable finned missile

$$0 \leq \tau \leq 1.0 \text{ and } -\infty \leq s \leq 0$$

Also for a statically stable finned missile, it can be seen from Equation (11) that

a. $(C_{Mq} + C_{M\dot{\alpha}})$ damps both the nutation and precession arms, assuming $(C_{Mq} + C_{M\dot{\alpha}}) < 0$.

b. A positive $C_{Mp\beta}$ tends to undamp the nutation arm and damp the precession arm.

c. A negative $C_{Mp\beta}$ tends to damp the nutation and undamp the precession.

Dynamic stability of a rolling finned missile requires that

$$\left| \frac{(C_{Mq} + C_{M\dot{\alpha}})}{2I} (1 - \tau) \right| > \left| C_{Mp\beta} \frac{\tau}{I_x} \right| \quad (15)$$

The aeroballistic theory was fit to the angular data from the wind tunnel by a least squares procedure using the WOBBLE computer program from Reference 5. The data were fit to the linearized theory in overlapping sections, yielding the parameters K_N , K_P , ω_N , ω_P , λ_N , and λ_P as functions of time.

The aerodynamic coefficients were computed from these parameters as follows:

For the three-degrees-of-freedom (3-D) case

$$C_{M\alpha} = \omega_N \omega_P \left(\frac{4I}{\pi Q d^3} \right) \quad (16)$$

$$(C_{Mq} + C_{M\dot{\alpha}}) = (\lambda_N + \lambda_P) \frac{8IV}{\pi Q d^4} \quad (17)$$

$$C_{Mp\beta} = - \left[\frac{\lambda_N \omega_P + \lambda_P \omega_N}{\omega_N + \omega_P} \right] \frac{8I_x V}{\pi Q d^4} \quad (18)$$

For the one-degree-of-freedom (1-D) case

$$C_{M\alpha} = -\omega^2 \left(\frac{4I}{\pi Q d^3} \right) \quad (19)$$

$$(C_{Mq} + C_{M\dot{\alpha}}) = \lambda \frac{16IV}{Q d^4} \quad (20)$$

The sign convention used for the coefficients is shown in Figure 4. Diagrams of the typical motions for the N-vane 1 configuration is shown in Figures 5 through 7. For a statically stable missile, the nutation arm (K_N) rotates in the same direction that the missile is spinning, while the precession arm (K_P) rotates in the opposite direction.

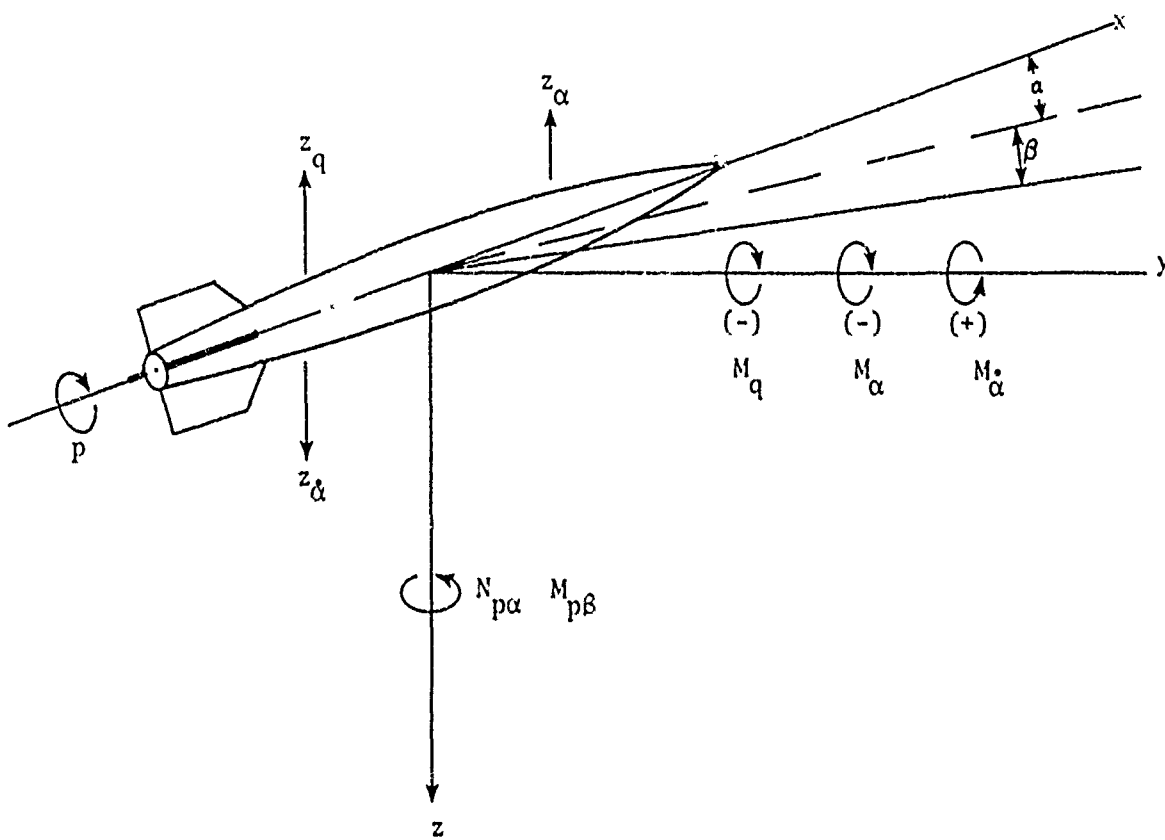


Figure 4. Force and Moment System

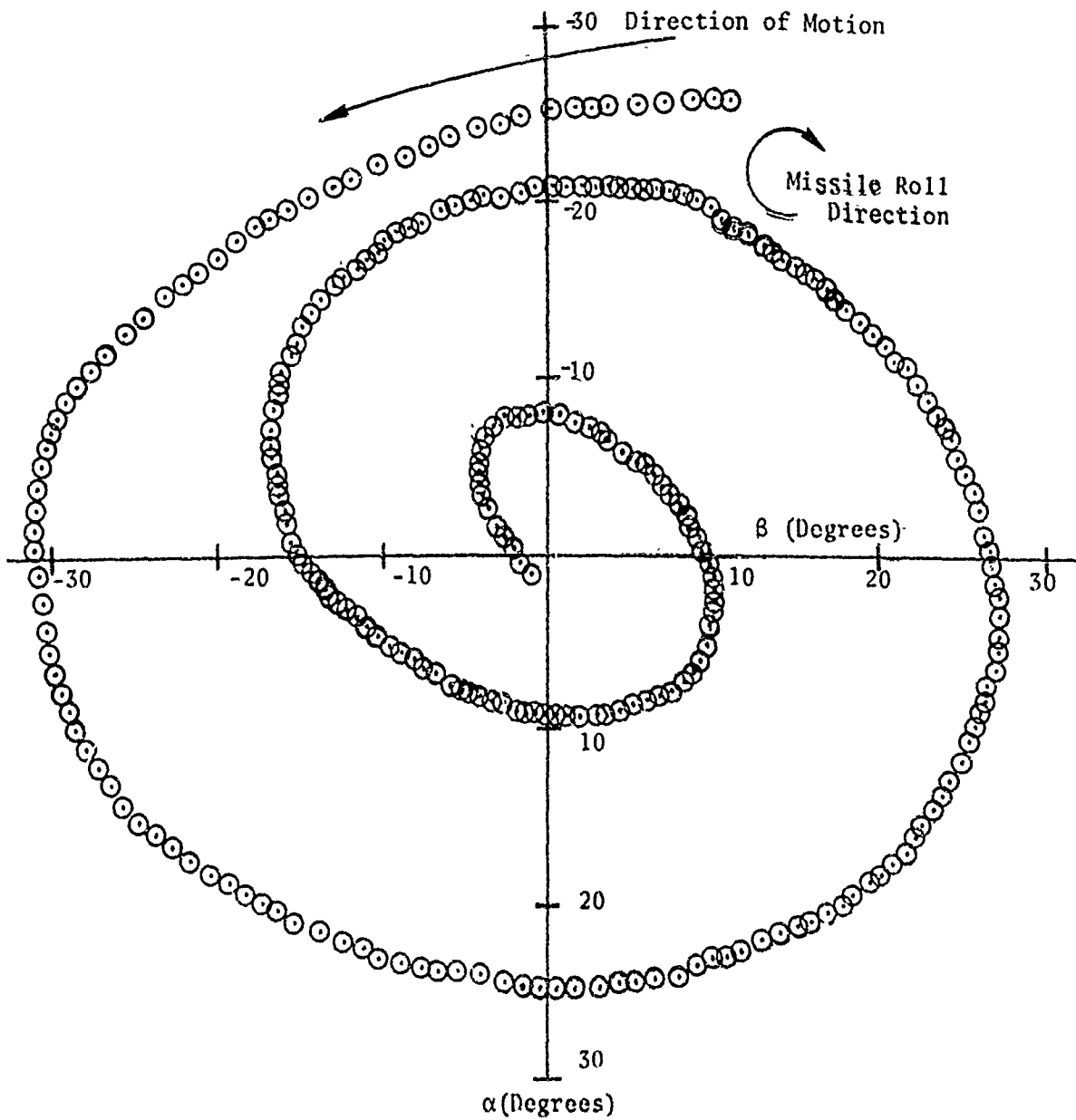


Figure 5. Example of 3-D Angular Motion (N-Vanes 1)

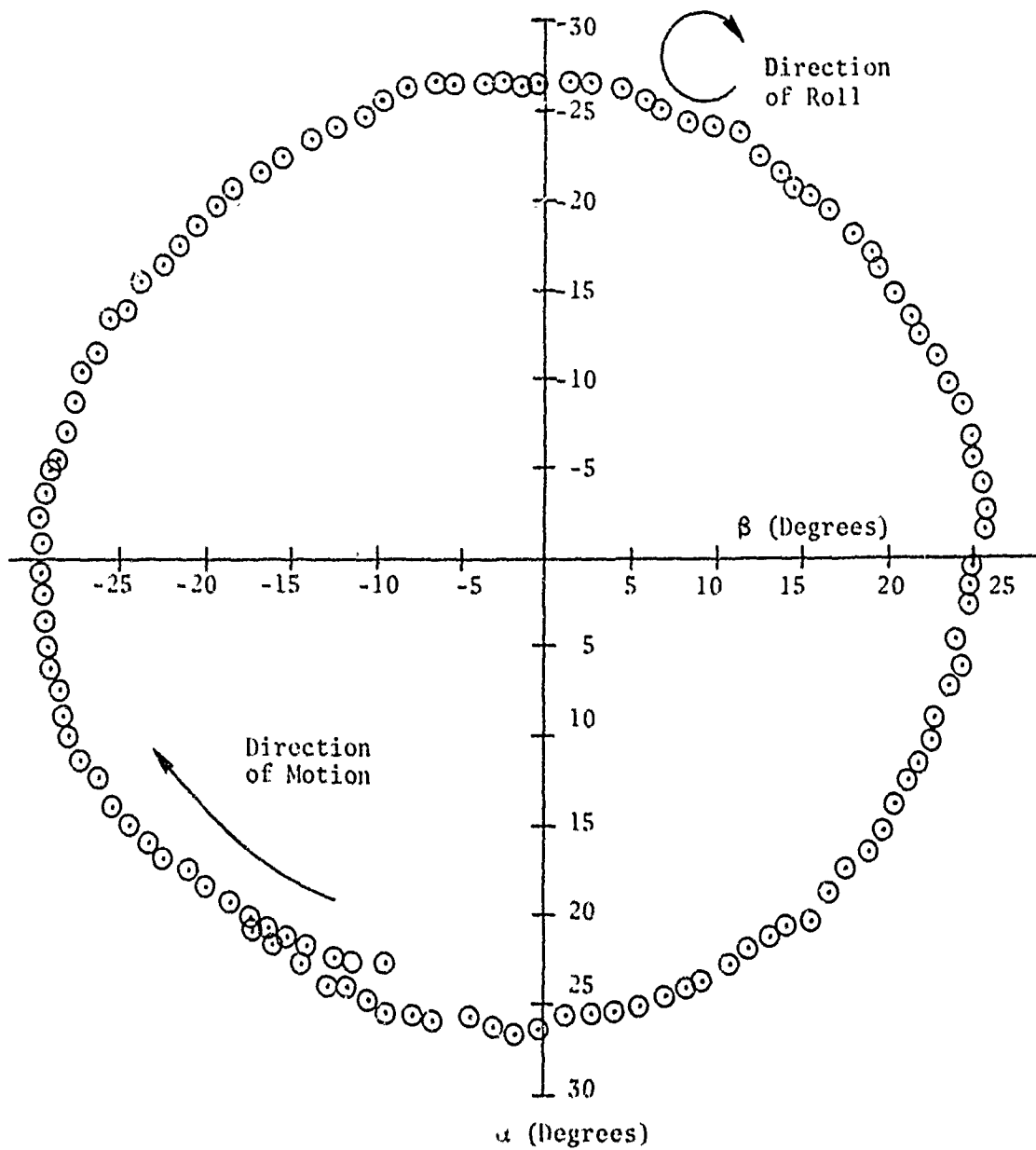


Figure 6. Nutation Limit Cycle (N-Vane 1) Configuration

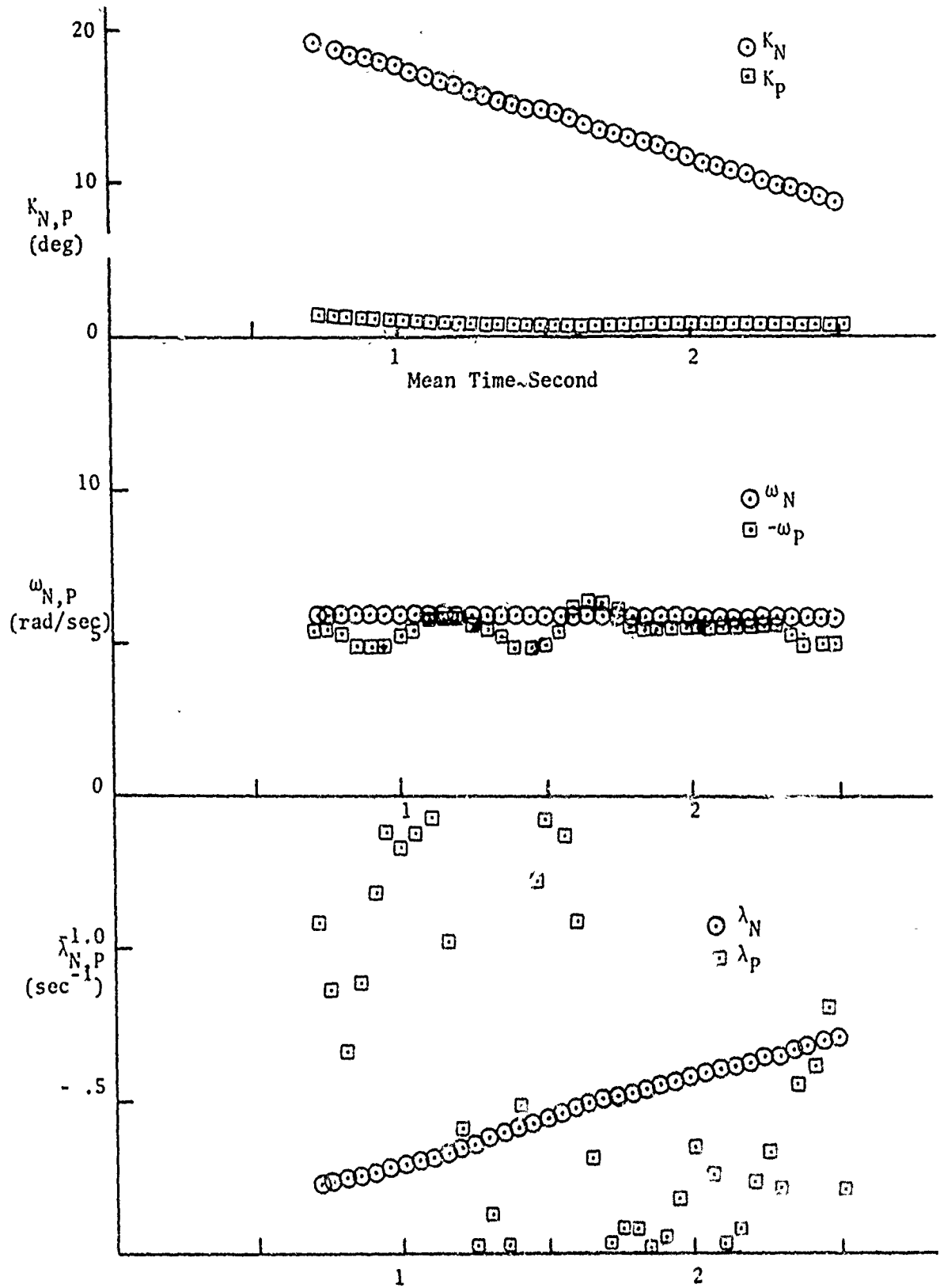


Figure 7. Data From N-Vane 1 Configuration (Run 1)

SECTION III

EXPERIMENTAL TECHNIQUE

The model tested was a low drag finned configuration (Figure 1 and Table I).

1. INERTIA MEASUREMENT

The torsion pendulum method (Reference 6) was used to determine the transverse and axial moments of inertia, I and I_x , for the model. In this technique, the model was supported by a 5-inch long, 0.037-inch diameter wire. The model was given an angular displacement and released, and periods were then averaged over a 10-cycle oscillation. The moments of inertia were computed using the measured periods and the spring constant of the wire.

2. WIND TUNNEL TESTING PROCEDURE

The Notre Dame low turbulence wind tunnel with a 2 by 2 foot test section was used for the 1-D, 3-D, and smoke flow tests as described in References 2 and 6. All the tests were run at a wind tunnel velocity of approximately 57 feet per second.

The model support system shown in Figure 8 was used for both 1-D and 3-D tests. This support system allowed the model to pitch freely on two sapphire jewel bearings and simultaneously to yaw on a sapphire cup. Rolling motions were obtained by allowing the front and rear sections of the model to rotate while the middle section of the model was free to pitch and yaw but not roll. The support system was mounted on the floor of the test section.

3. 1-D WIND TUNNEL TESTING PROCEDURE

For the 1-D tests, the clean configuration (Figure 9a) was used. The model was fixed on the support system so that it was not free to pitch or roll.

To obtain the 1-D yawing motion in the wind tunnel, a moving camera technique was used. This technique consisted of a still camera, with its shutter open, propelled along a stationary track. The wind tunnel setup is shown in Figure 10. The model was illuminated by a strobe light flashing at intervals of 0.068 second.

4. 1-D DATA REDUCTION PROCEDURE

The 1-D angular oscillations were converted to digital values of angle of attack by using an optical comparator to measure the displacement of the nose as a function of time and a computer program to convert this information

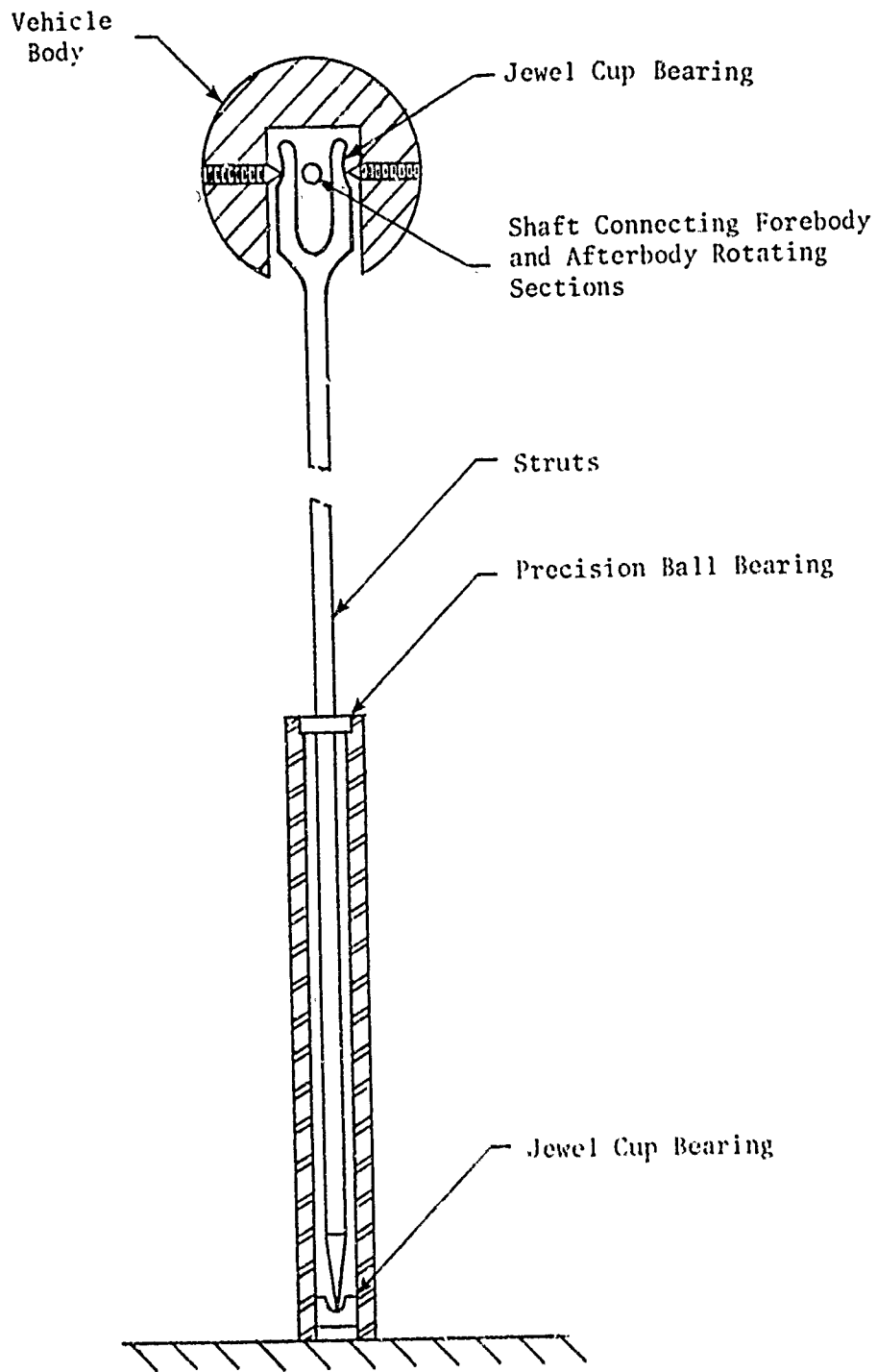
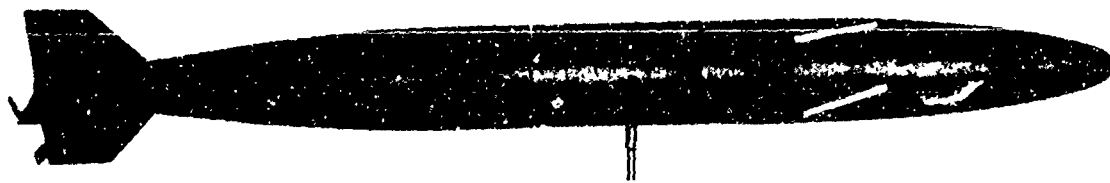


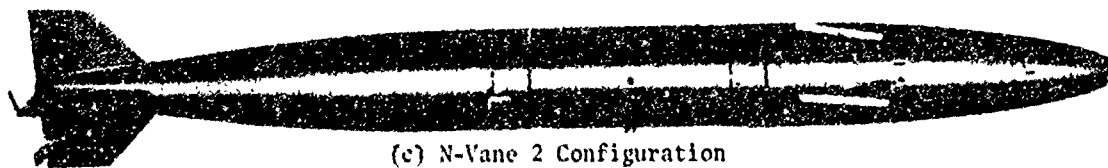
Figure 8. 3-D Support System



(a) Clean Configuration



(b) N-Vane 1 Configuration



(c) N-Vane 2 Configuration

Figure 9. Wind Tunnel Test Models

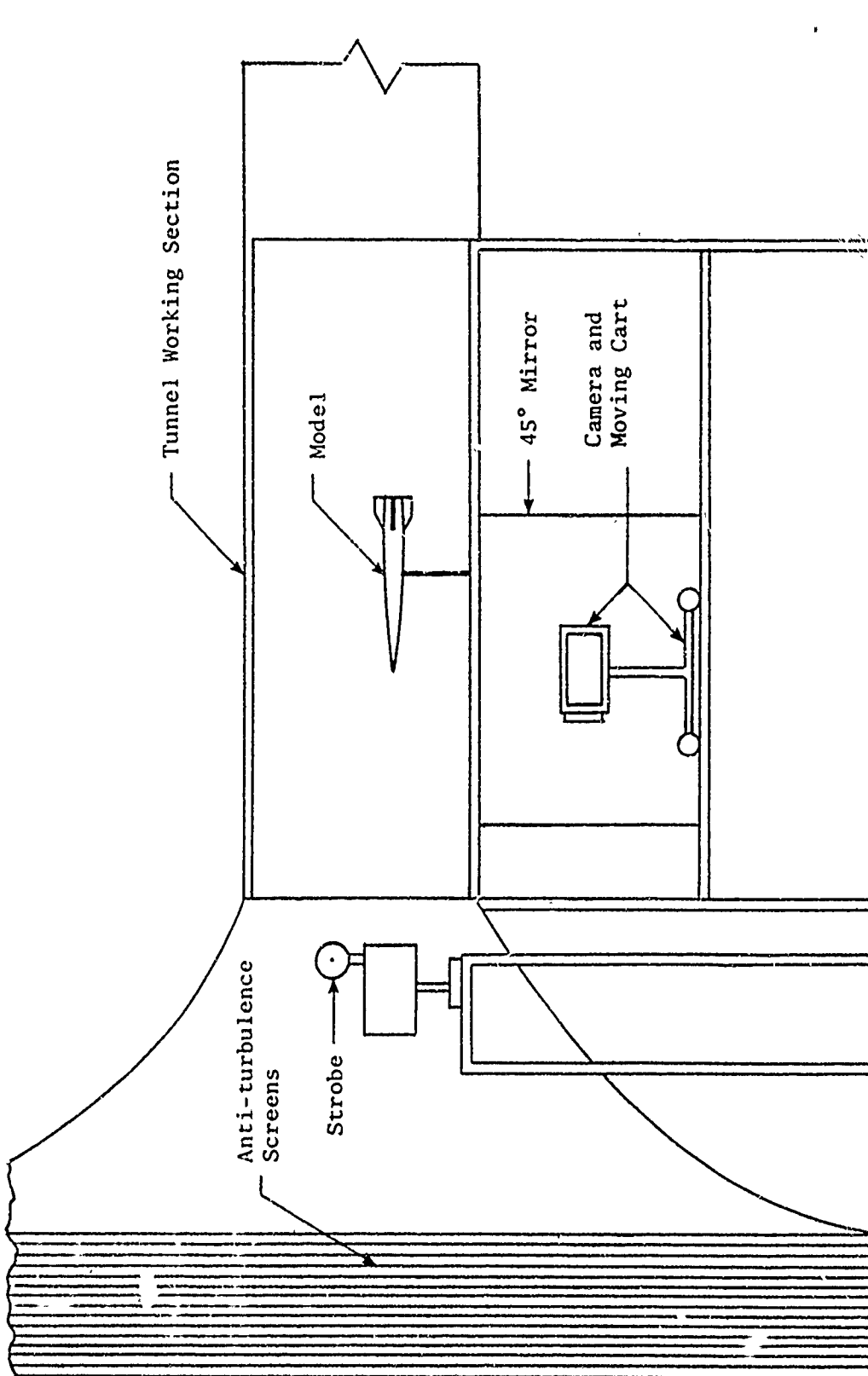


Figure 10. 1-D Test Set-Up

TABLE I. PHYSICAL CHARACTERISTICS OF TEST MODEL

Mass, slugs	0.0766
Axial moment of inertia, slug-ft ²	0.000218
Transverse moment of inertia, slug-ft ²	0.00569
Model length, inches	22.25
Model diameter, inches	2.0
Center of gravity, inches from nose	10.12

to angular data. Two reference marks were painted on a rod inserted into the wind tunnel as shown in Figure 11. The distance between the two marks was used for converting picture distances to angular data.

5. 3-D WIND TUNNEL TESTING PROCEDURE

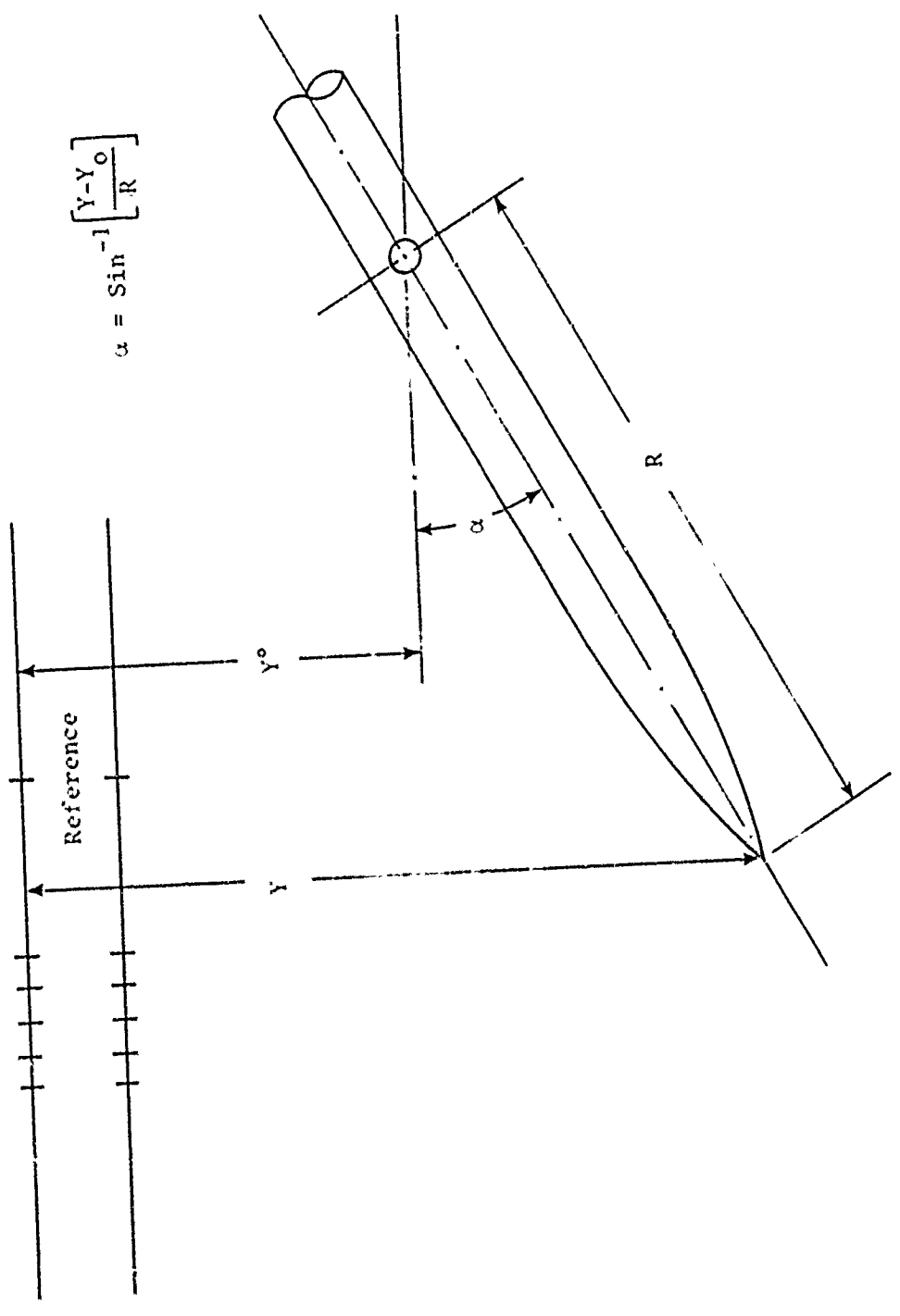
For the 3-D tests, the model was made to spin at steady state roll rates from 20 to 60 rad/sec by adding small tabs (Figure 9(b) and 9(c)). To obtain 3-D angular motions for reduction to aerodynamic coefficients, the model was given an initial angle of attack and angular rate. The subsequent motions were recorded using a Millikan camera running at 128 frames per second. A first-surface mirror was mounted at the rear of the test section at a 45-degree angle to both the model and the camera. This test setup is shown in Figure 12 and described in Reference 7.

6. 3-D DATA REDUCTION PROCEDURE

The 3-D angular motion was converted to angle of attack and angle of sideslip from the motion pictures using an optical comparator and a computer program. Two reference marks were painted on a thin rod inserted into the wind tunnel from the bottom. Reference marks were also painted on the rear of the missile and on one of the missile fins. This reference point system is shown in Figure 13. The distance between the two reference marks on the rod were measured and used as a scale factor for converting from picture units to wind tunnel units. The distance from the center of gravity of the model to the rear reference mark was also measured. This measurement provided information for converting from comparator readings to angle of attack and angle of sideslip (Figure 14). Roll rate data were obtained by taking an average of the time required for the dot on the fin to make ten revolutions. The roll rate was nearly constant throughout each test.

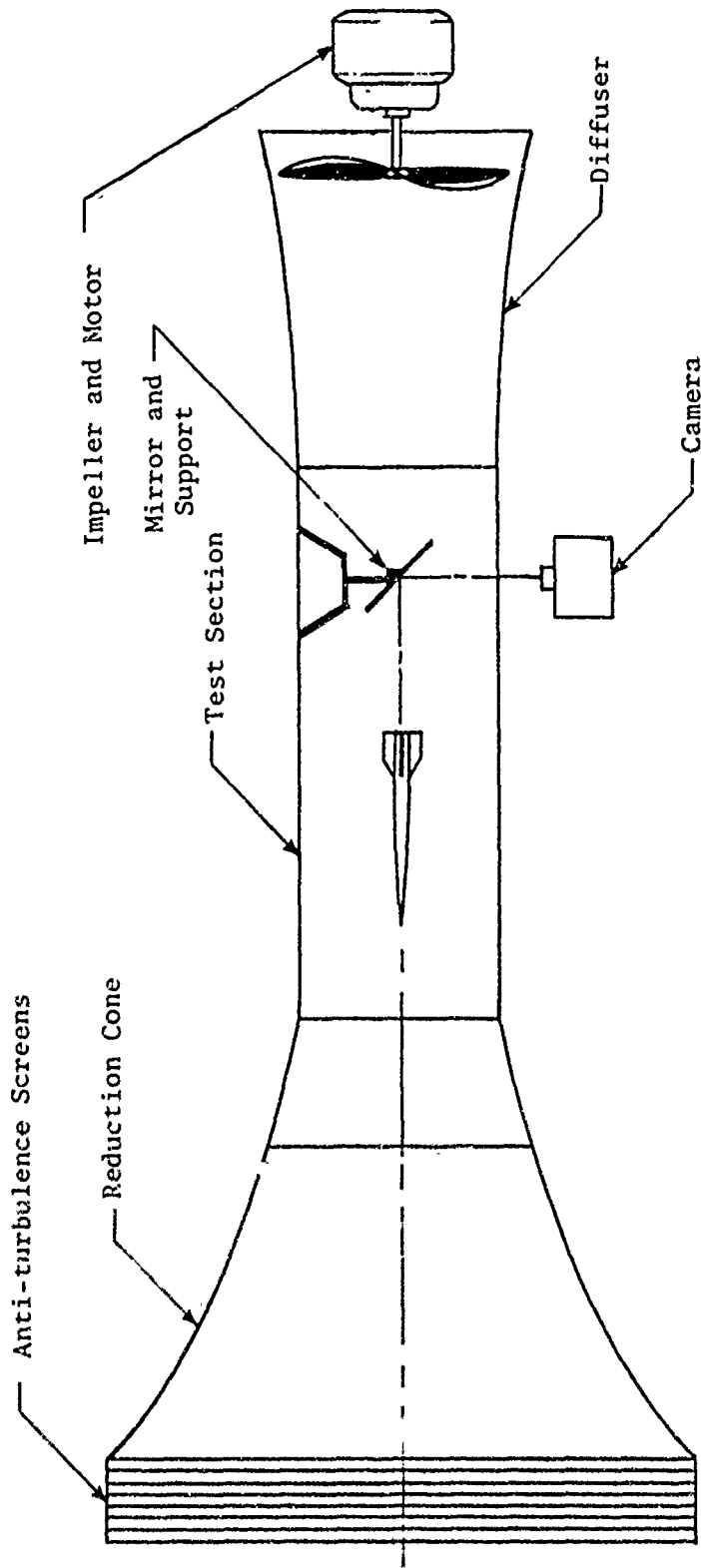
7. FLOW VISUALIZATION TECHNIQUE

The flow visualization equipment used is described in Reference 8. Smoke was produced in a smoke generator in which kerosene dripped onto electrically heated plates. The smoke was introduced in the low turbulence tunnel ahead of anti-turbulence screens. The velocity in this region was about 1 ft/sec. The velocity in the test section was 57 ft/sec.



$$\alpha = \sin^{-1} \left[\frac{Y - Y_0}{R} \right]$$

Figure 11. 1-D Data Reduction Procedure



TOP VIEW

Figure 12. 3-D Wind Tunnel Set-Up

WIND TUNNEL TEST SECTION

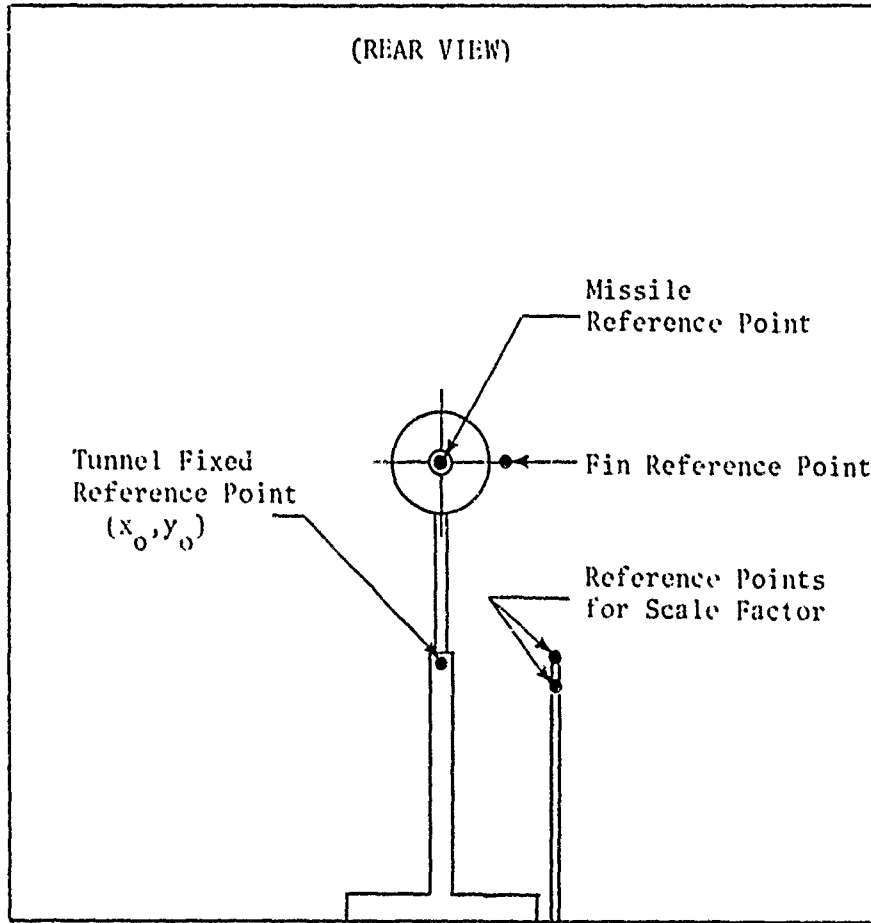
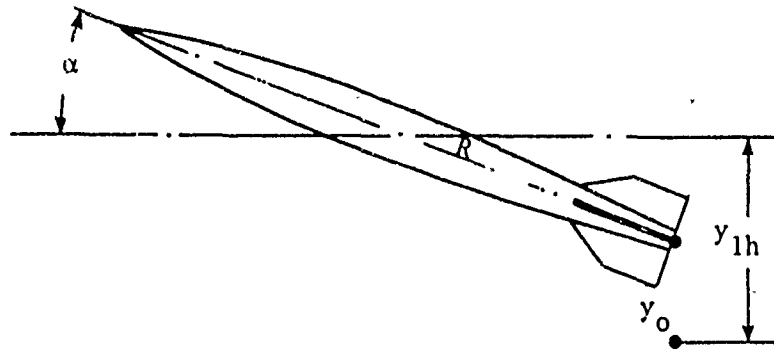


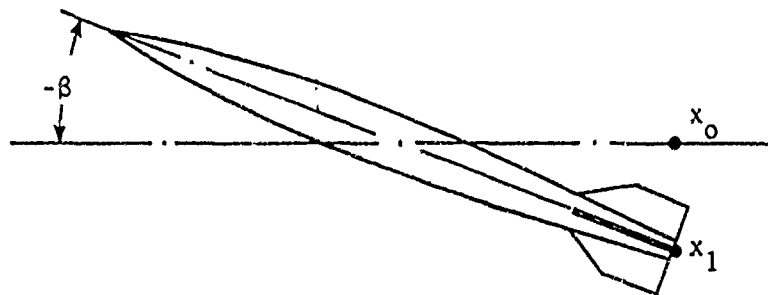
Figure 13. 3-D Reference Point System

SIDE VIEW



$$\alpha = \text{Sin}^{-1} \left[\frac{h - (y_1 - t_0) * \text{SF}}{R} \right]$$

TOP VIEW



$$\beta = \text{Sin}^{-1} \left[\frac{(x_1 - x_0) * \text{SF}}{R} \right]$$

Figure 14. Reduction of Tunnel Motion to Angular Data

SECTION IV

RESULTS

The primary objective of this test program was to determine if a Magnus instability of a finned configuration could be eliminated by adding N-vanes to the model.

An investigation was initially undertaken to observe the 3-D angular motions possible with the clean configuration. It was found that the clean configuration could be easily put into a precession limit cycle (angular motion in opposite direction of spin) of approximately 35 degrees amplitude, when initially excited in the precession mode. This limit cycle motion was obtained over a large range of spin rates. When excited in the nutation mode, the model damped to zero angle of attack.

Various N-vanes were attached to the model as shown in Figure 2 to determine if the precession limit cycle could be eliminated. It was found that N-vanes on the rear half of the model had little noticeable effect on the motion of the missile.

Adding the N-vanes to the nose had a marked effect on the motion. The N-vane configuration shown in Figure 2(b) (N-vane 1) completely eliminated the precession limit cycle and created a nutation limit cycle (angular motion in same direction as spin) of about 25 degrees amplitude, when excited in the nutation mode.

The N-vane configuration shown in Figure 2(c) (N-vane 2) eliminated both the precession and nutation limit cycles for all initial angles of attack and angular rates.

SECTION V

ANALYSIS OF DATA

Data from the 1-D test were obtained from the clean configuration, and the coefficients $C_{M\alpha}$ and $(C_{Mq} + C_{M\dot{\alpha}})$ are plotted in Figures 15 and 16. The 1-D yawing motion damped out rapidly, and as a result, the highest mean angle of attack for a section fit that could be obtained was 13.5 degrees. These data were very repeatable and are compared with the 3-D results in Figures 17(a) and 18(a). The 1-D and 3-D results compare relatively well over the angles of attack where both types of data were taken.

A summary of the 3-D data is presented in Table II and Figures 17 to 23. These data were taken at roll rates of approximately 50 rad/sec which were about eight times the missile nutation frequency. After the data were reduced to angles and were fit with the WOBBLE computer program, it became evident that almost all the motions were nearly circular and contained one large arm (K_N or K_P) and one small arm (K_N or K_P). For a section length of 1.3 cycles (about 170 data points), the WOBBLE fits gave good results for the λ and ω corresponding to the large arm and gave poor results for the λ and ω corresponding to the small arm (Figure 17) (N-vane 1, run 1). The motion in this run was almost pure nutation. The WOBBLE fit gave a well defined K_N , ω_N , and λ_N ; however, K_P was very small. The amplitude of K_P for this case was on the same order as the pitch and yaw residuals from the WOBBLE fit. The determination of ω_P from the fit was marginal, and λ_P was very poor. The values obtained for the coefficients $(C_{Mq} + C_{M\dot{\alpha}})$ and $C_{M\beta}$ contained so much scatter due to the bad determination of ω_P and λ_P that they were deemed useless. Several different section lengths of data were tried as well as various initial approximations to the fitting routine, and a numerical integration fitting routine, all without significant improvement. Similar results were obtained for most of the other runs.

Since some runs that contained pure nutation and others that contained pure precession were obtained for all the configurations, the ω_N and λ_N for the pure nutation runs were combined with the ω_P and λ_P from the pure precession runs to compute the coefficients $C_{M\alpha}$, $(C_{Mq} + C_{M\dot{\alpha}})$, and $C_{M\beta}$. This procedure worked very well except that twice as many runs were required to compute the coefficient as would have been the case if two arms had been present in each run. Also run-to-run variations in spin rate and velocity had to be neglected.

The values for ω_N , ω_P , λ_N , and λ_P are plotted in Figures 20 to 23. The angle of attack range that was of most interest was from 0 to 30 degrees, but the plots show gaps in the ω and λ data. Where no data were available, a line was faired through the existing data to obtain the trend. Values for $C_{M\alpha}$, $(C_{Mq} + C_{M\dot{\alpha}})$, and $C_{M\beta}$ (Figure 24) were computed from Equations (16), (17), and (18), and the ω and λ data were obtained as described. Where a two arm fit was possible, the coefficients are included on the plots. The dynamic damping factors are plotted on Figure 25 and the motion half lives are listed in Table III.

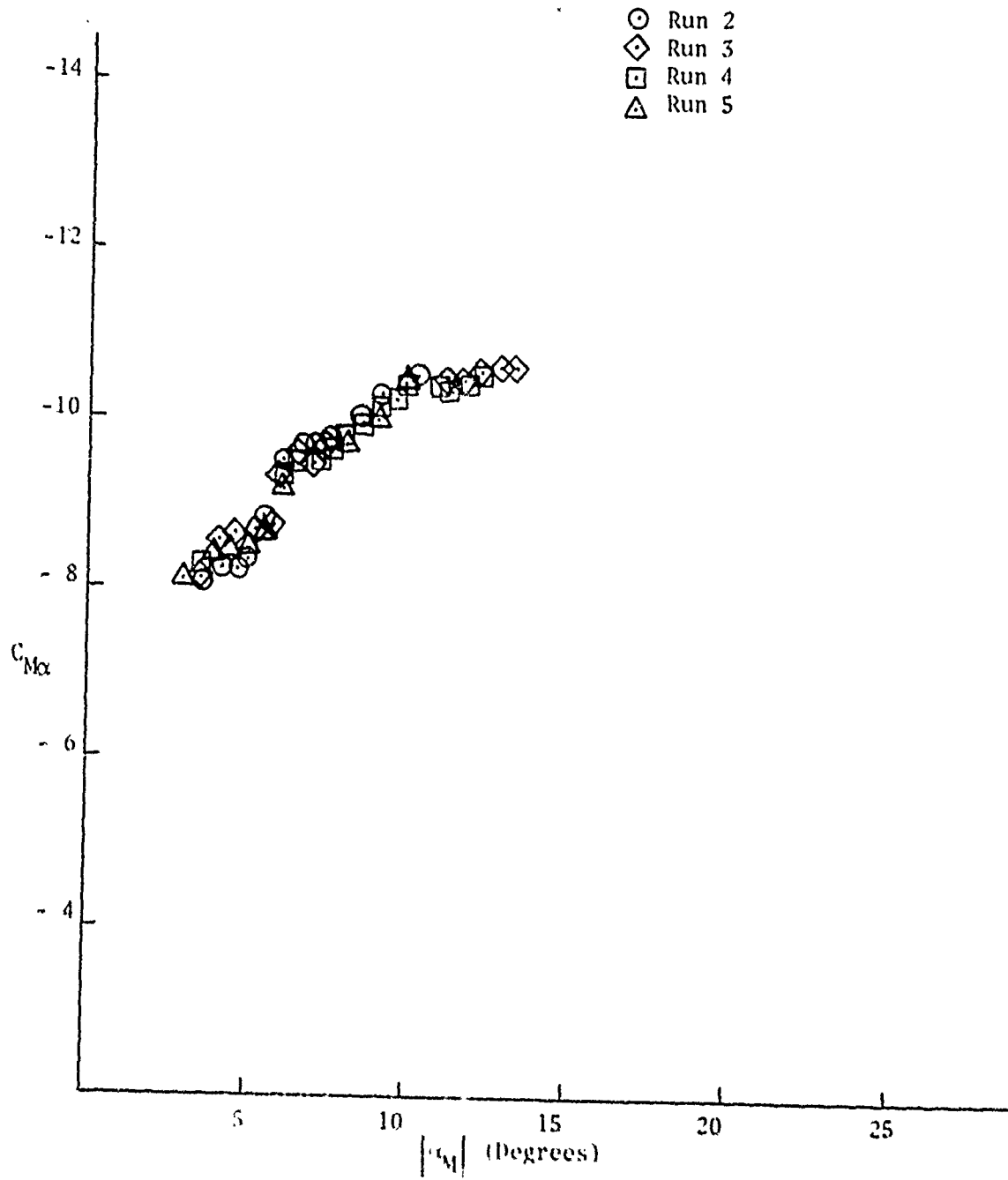


Figure 15. $C_{M\alpha}$ for Clean Configuration from 1-D Tests

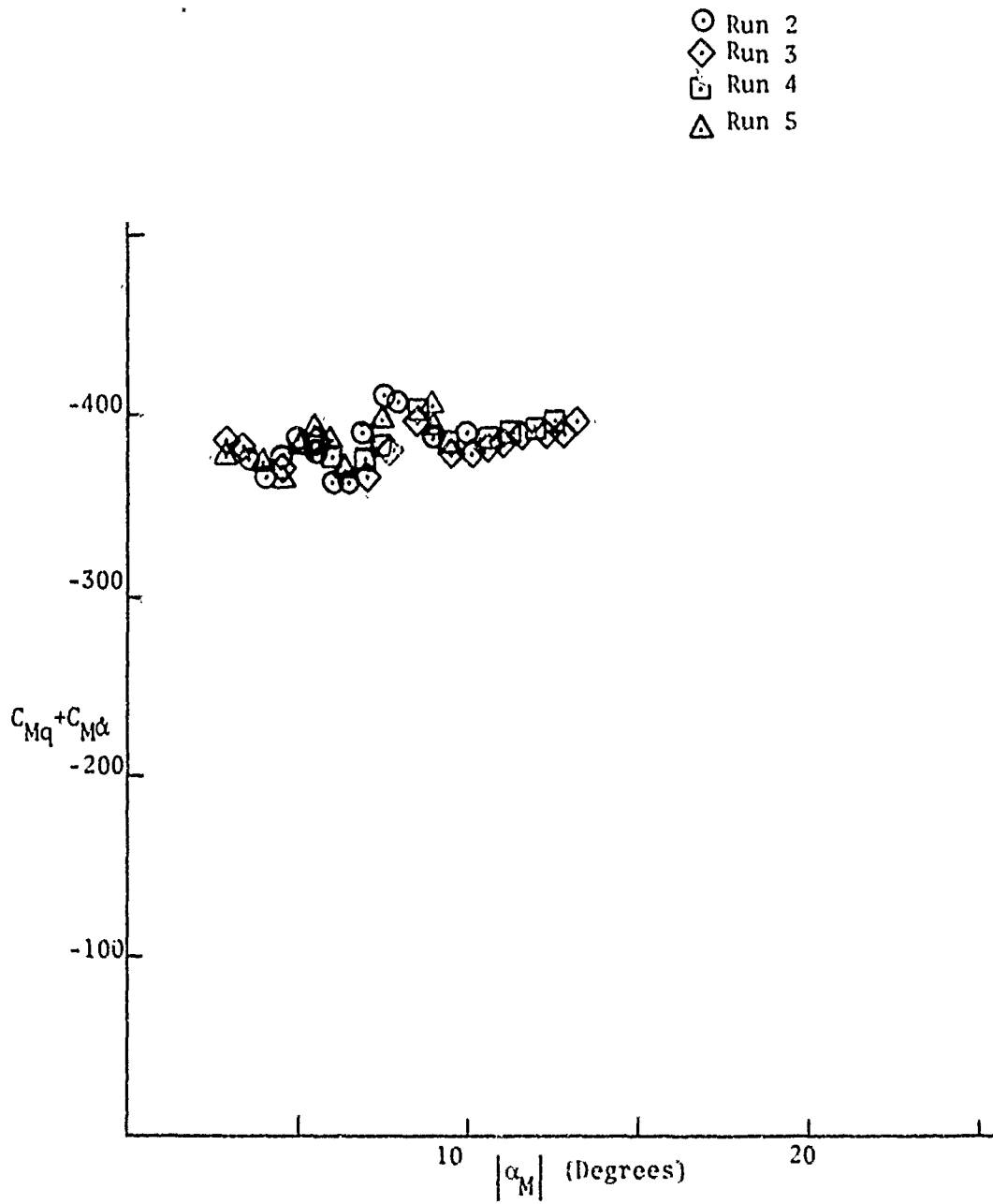


Figure 16. $(C_{Mq} + C_{M\alpha})$ for Clean Configuration from 1-D Tests

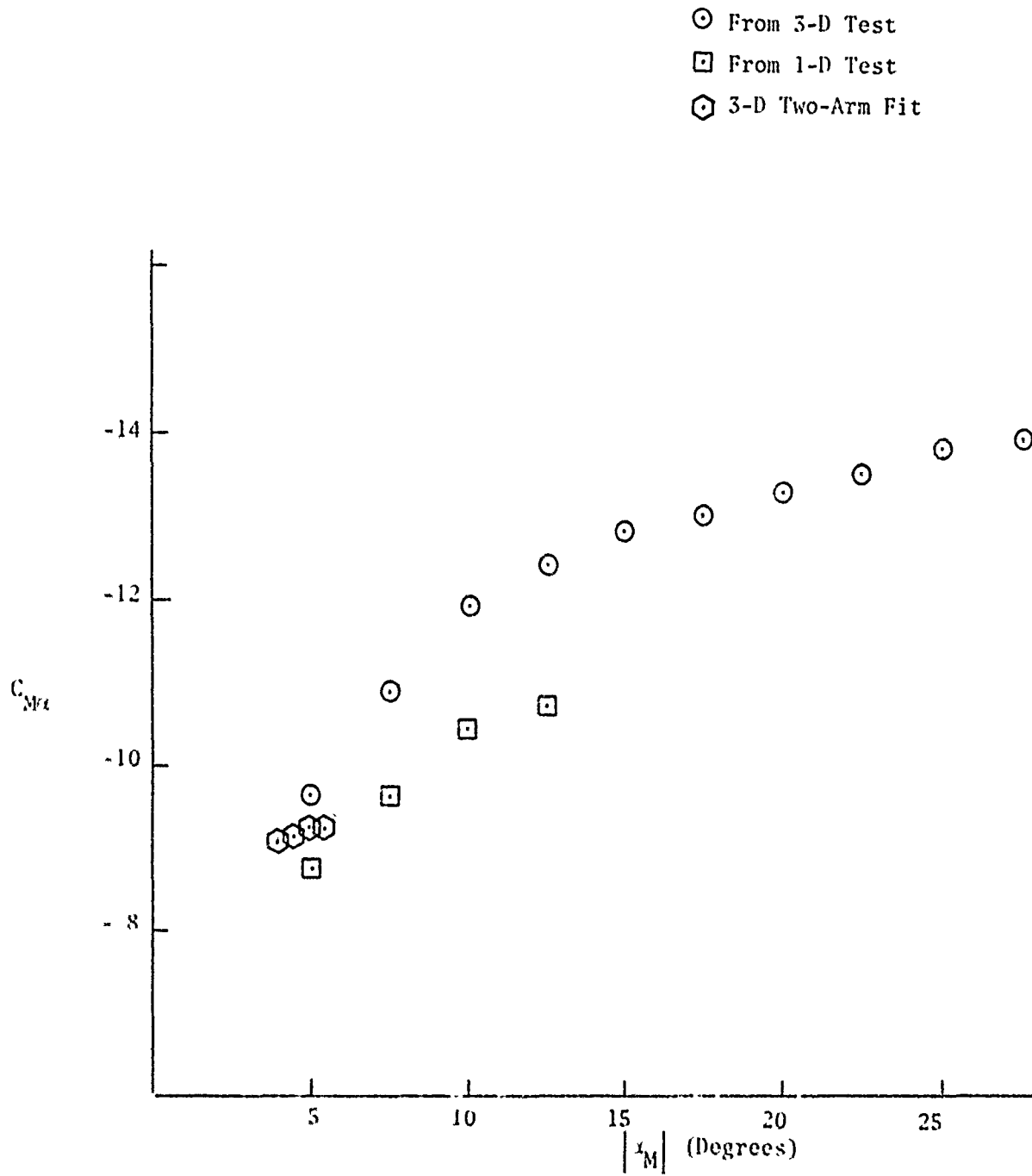


Figure 17 (a). Pitching Moment Coefficient for Clean Configuration

⊕ Two-Arm Fit

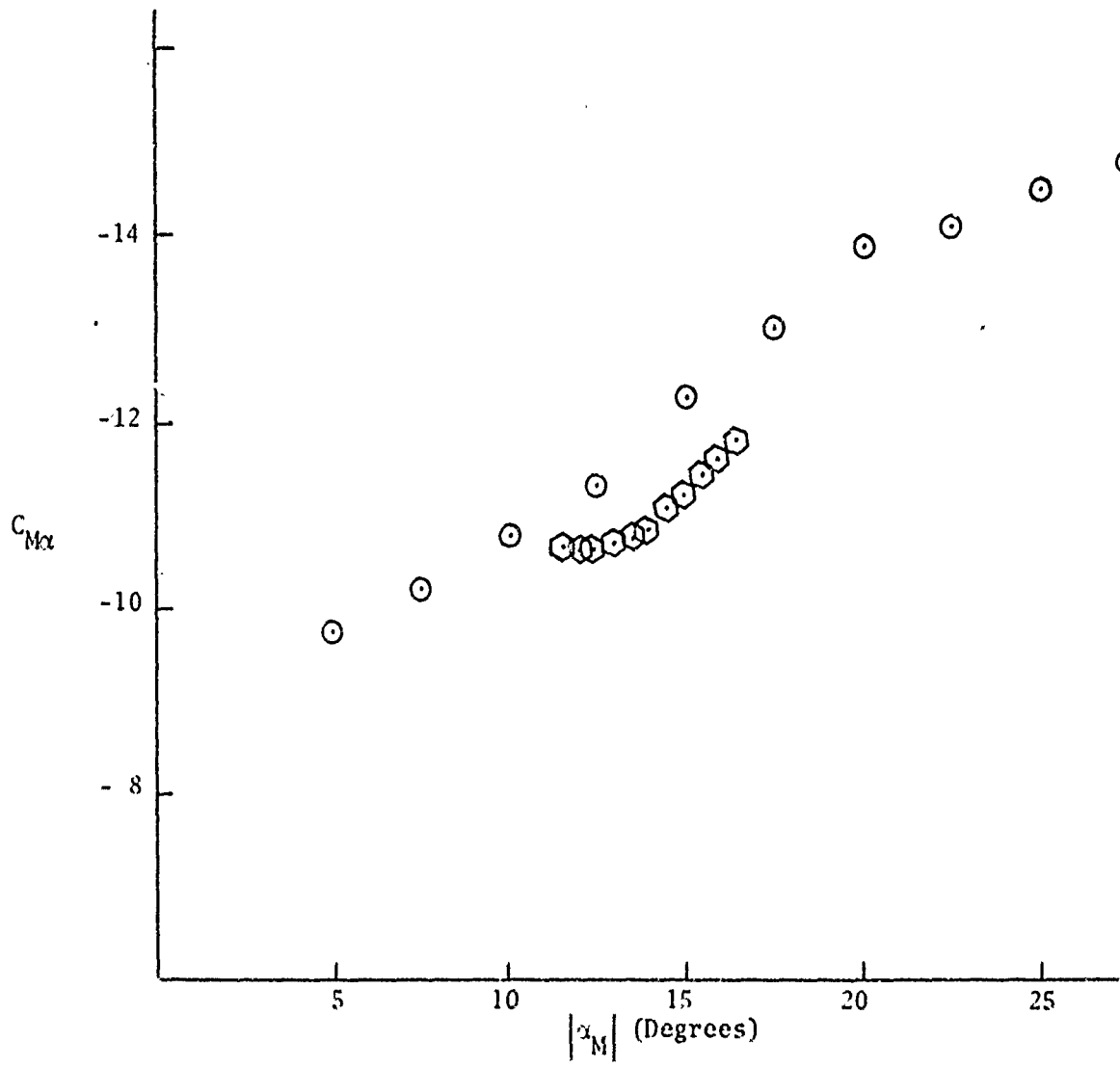


Figure 17 (b). Pitching Moment Coefficient for N-Vane 1 Configuration

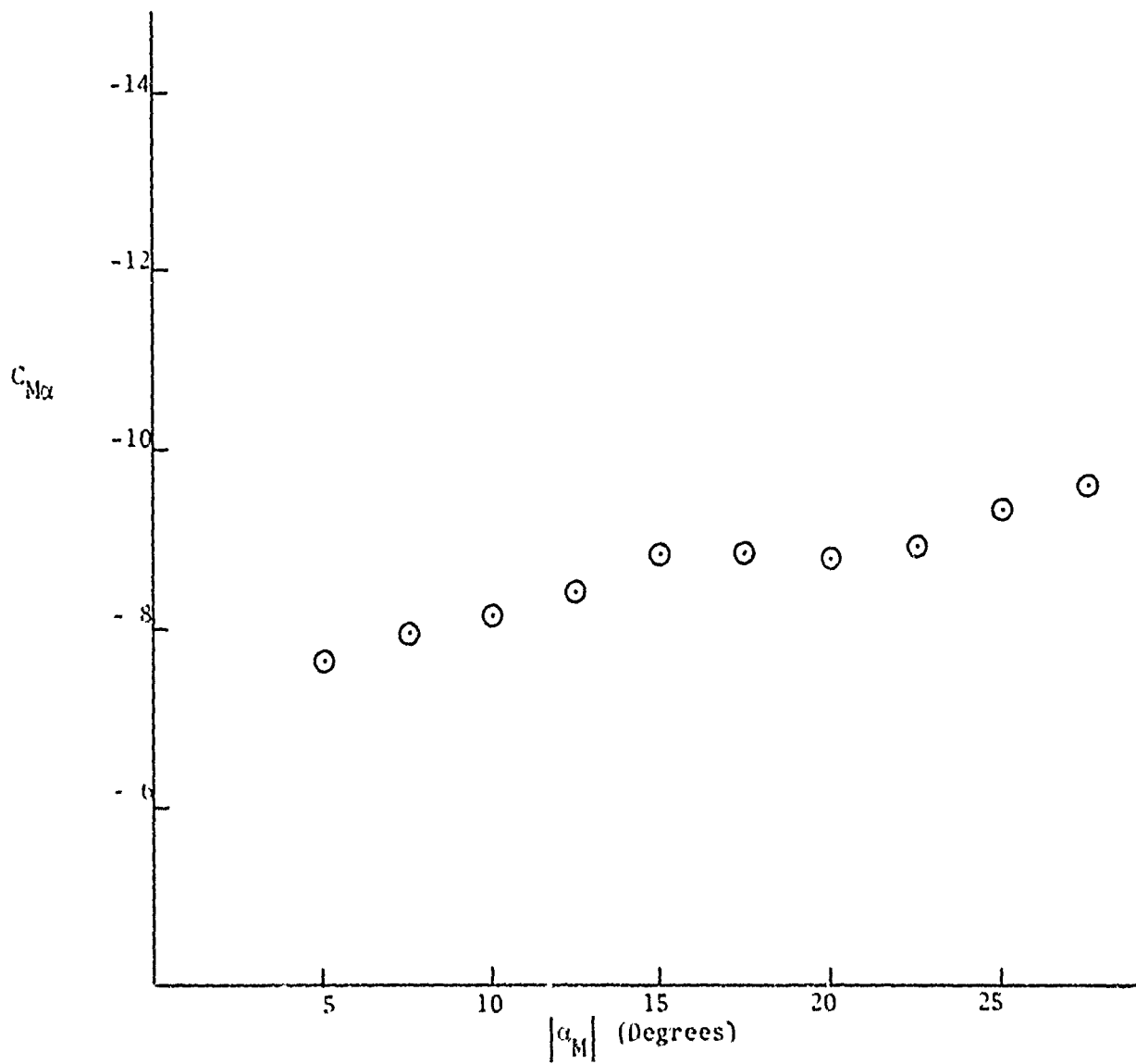


Figure 17 (c). Pitching Moment Coefficient for N-Vane 2 Configuration

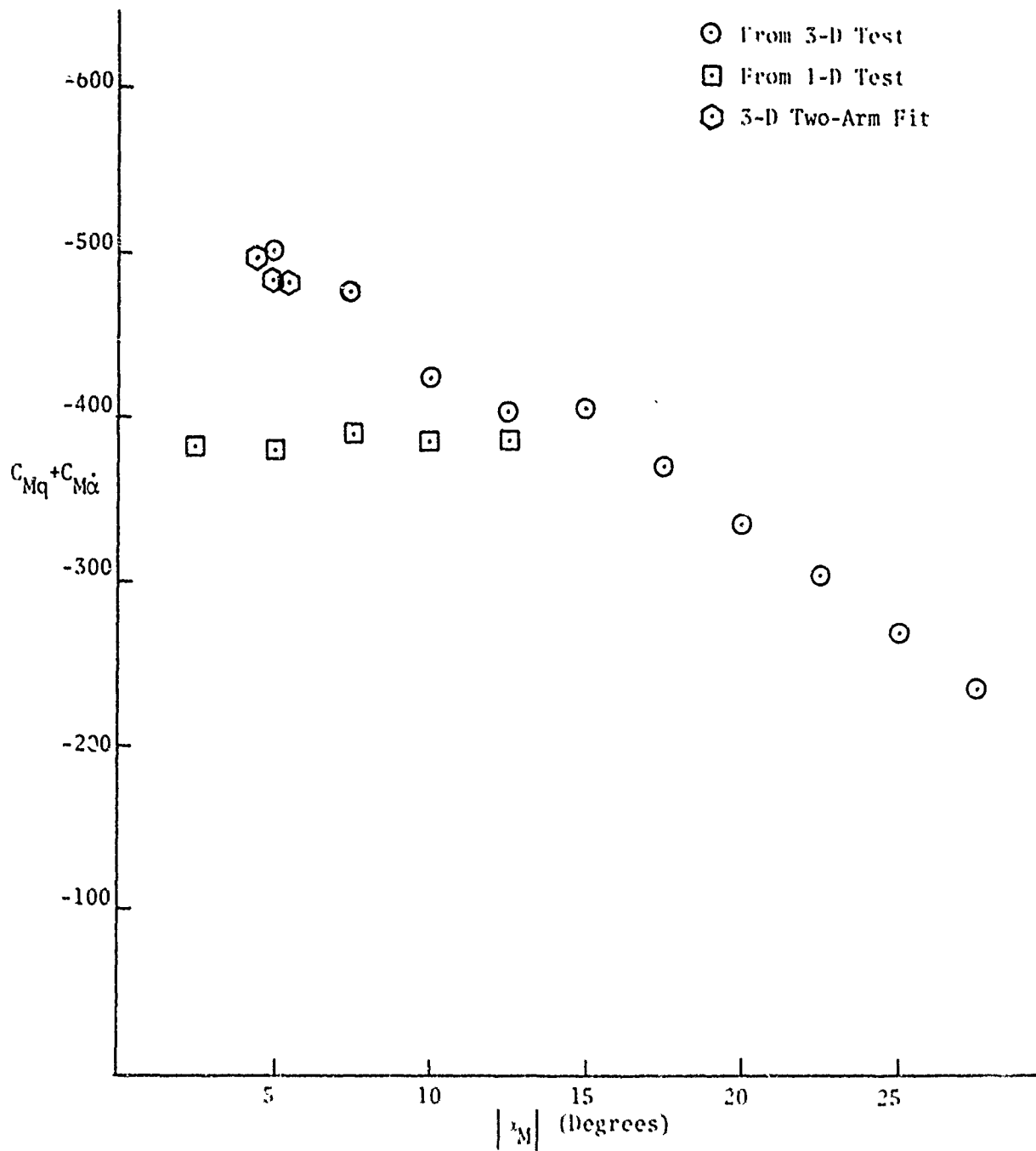


Figure 18 (a). Fitch Damping Moment Coefficient for Clean Configuration

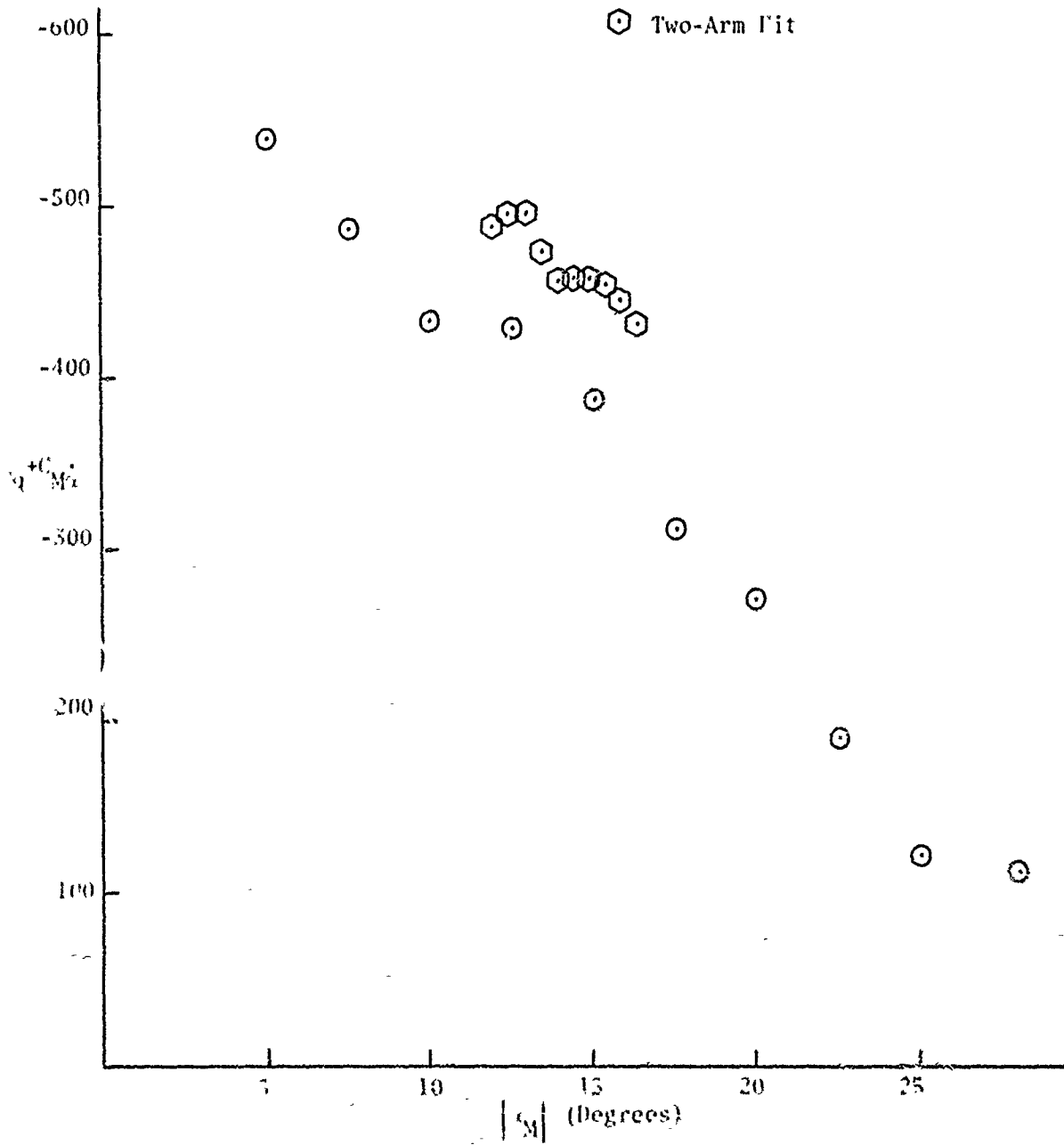


Figure 18 (b). Pitch Damping Moment Coefficient for N-Vane 1 Configuration

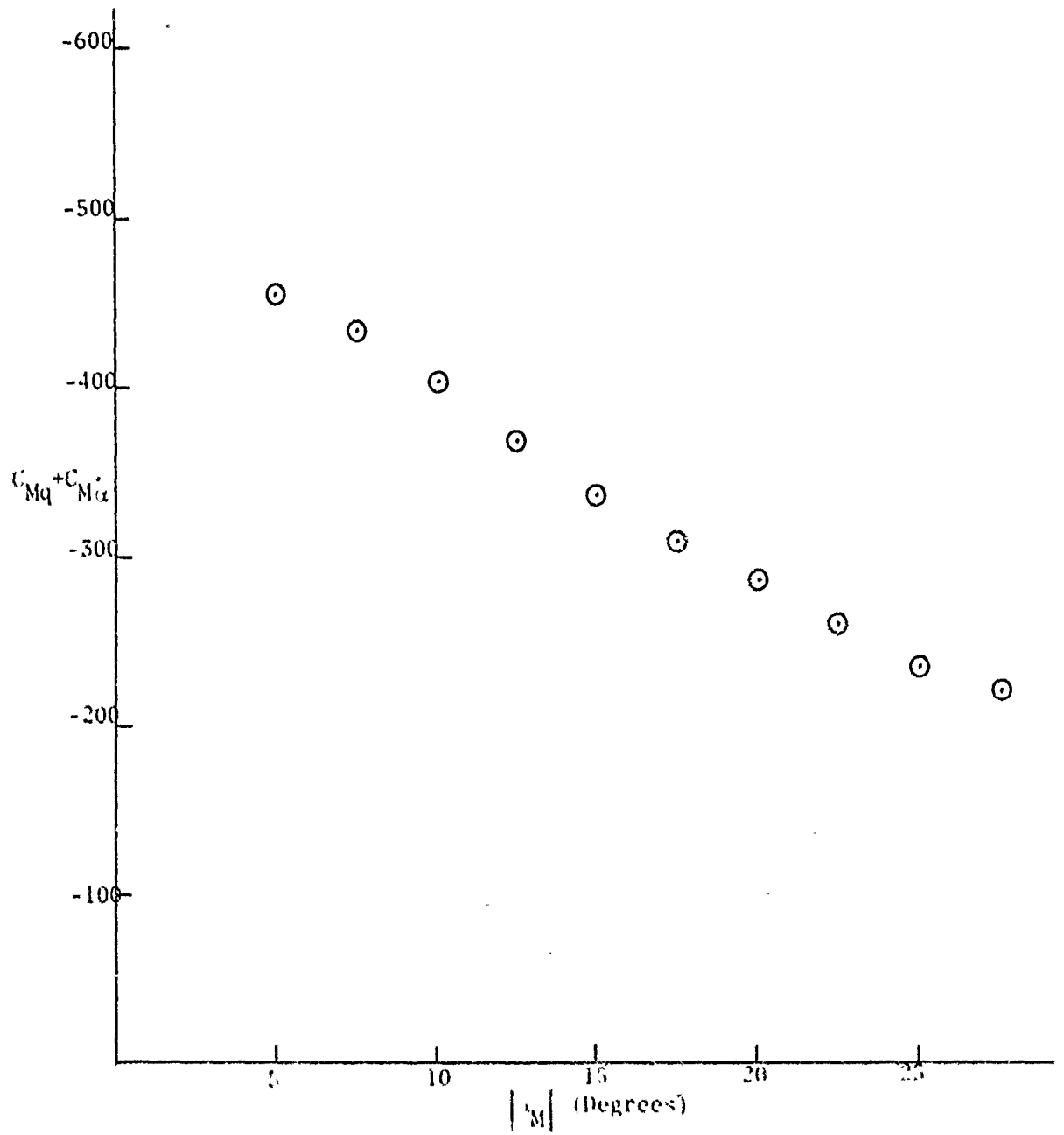


Figure 18 (c). Pitch Damping Moment Coefficient for N-Vane 2 Configuration

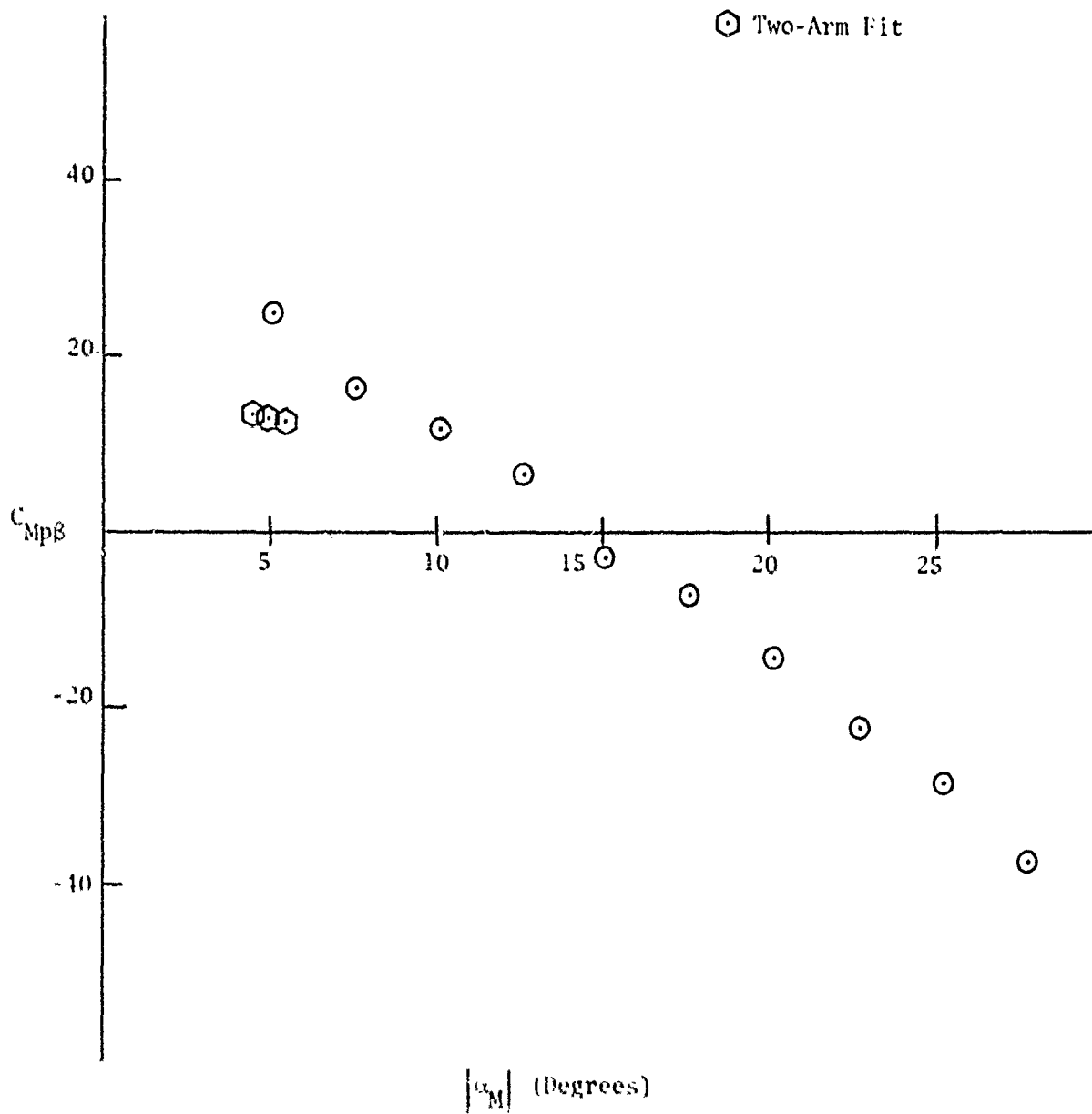


Figure 19 (a). Magnus Moment Coefficient for Clean Configuration

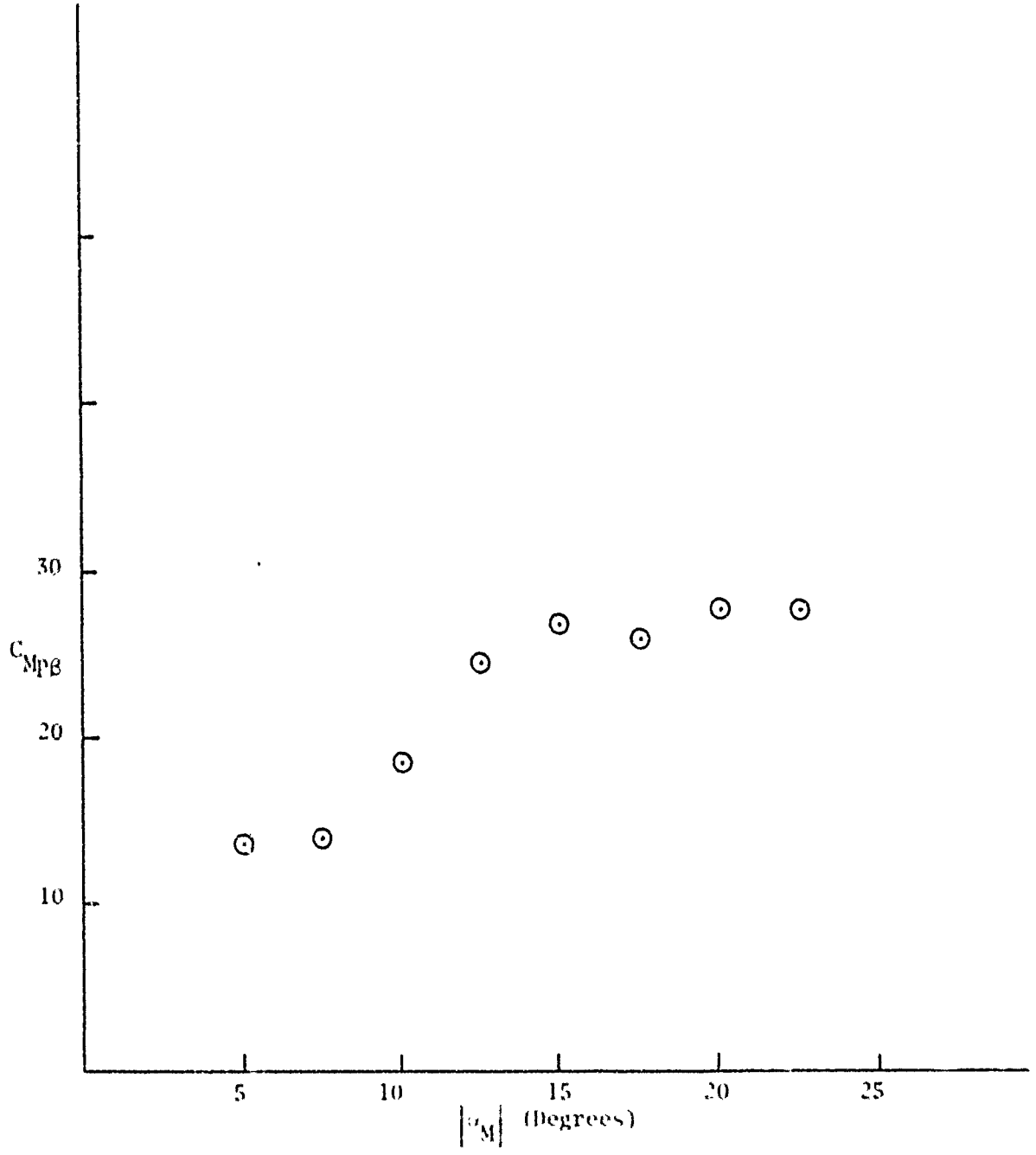


Figure 19 (b). Magnus Moment Coefficient for N-Vane 1 Configuration

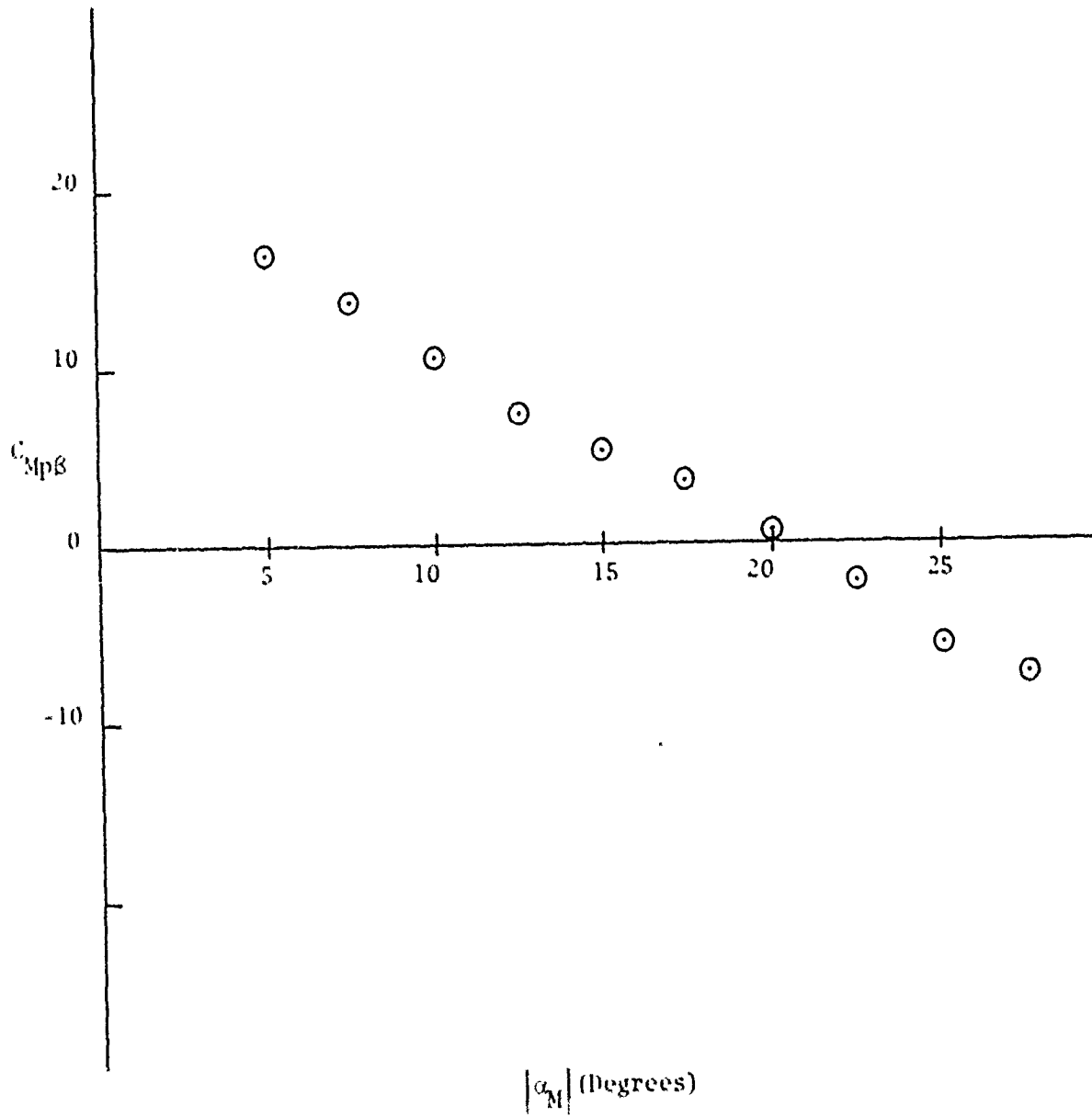


Figure 19 (c). Magnus Moment Coefficient for N-Vane 2 Configuration

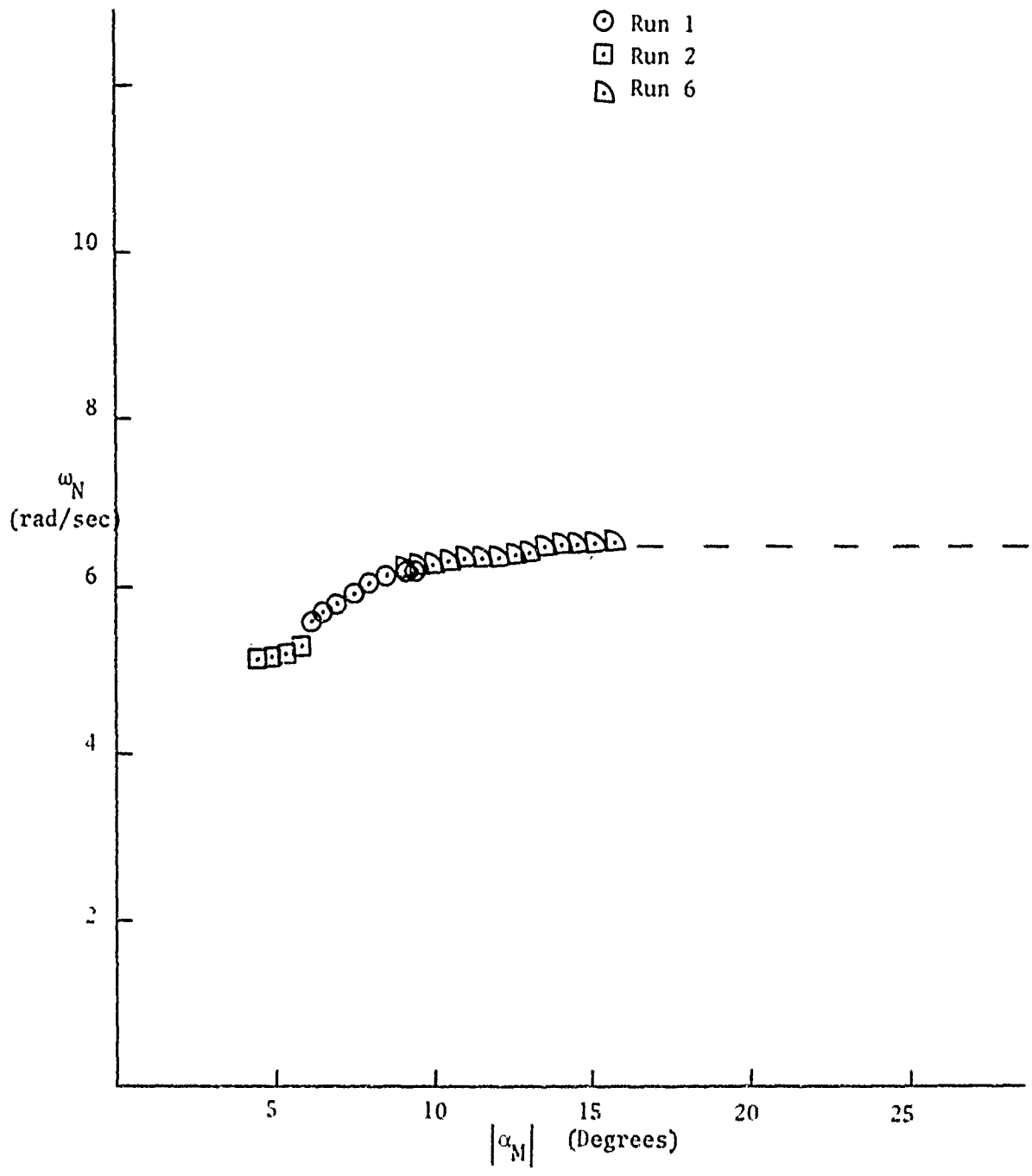


Figure 20 (a). Nutation Frequency for Clean Configuration from 3-D Test

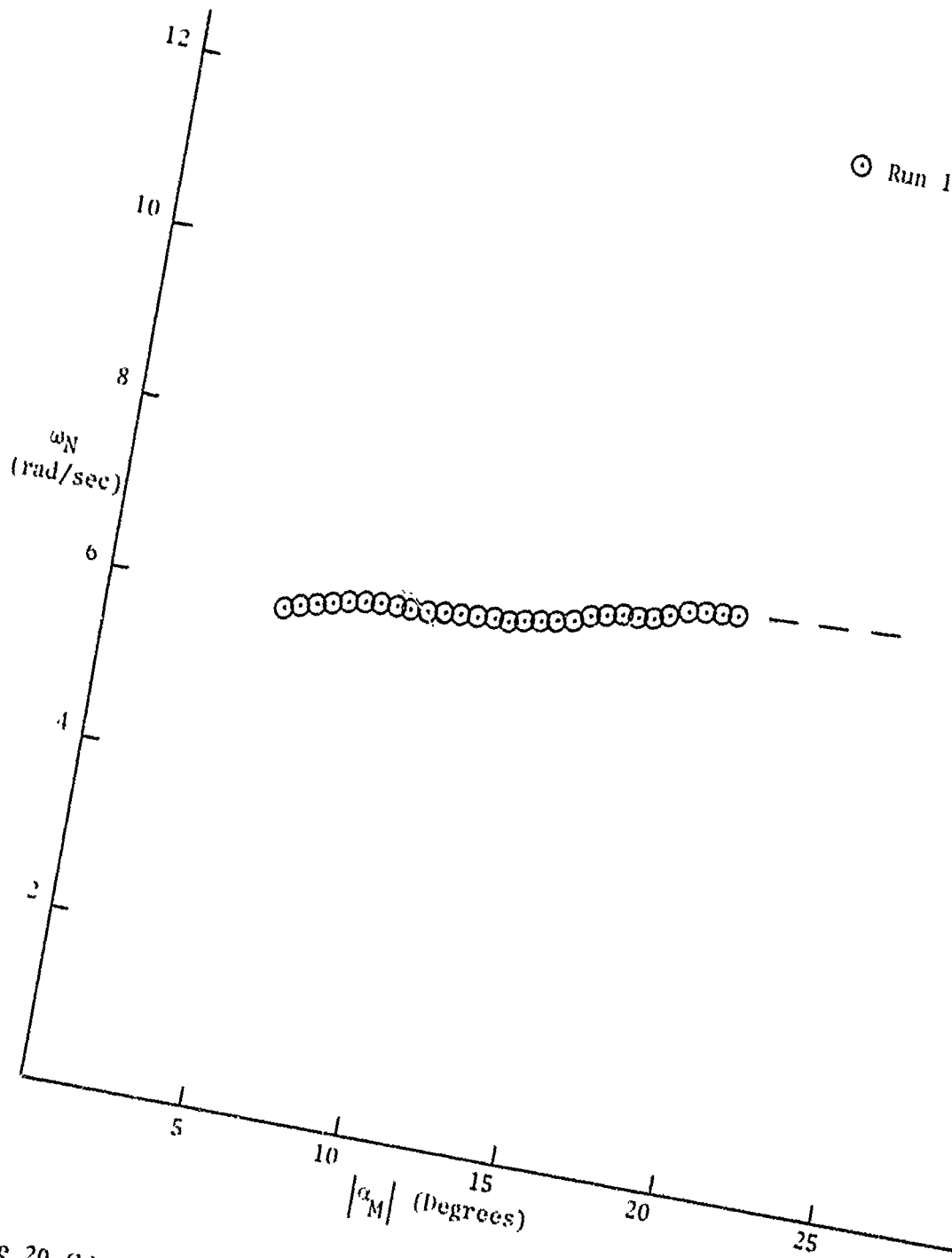


Figure 20 (b). Nutation Frequency for N-Vane 1 Configuration from 3-D Test

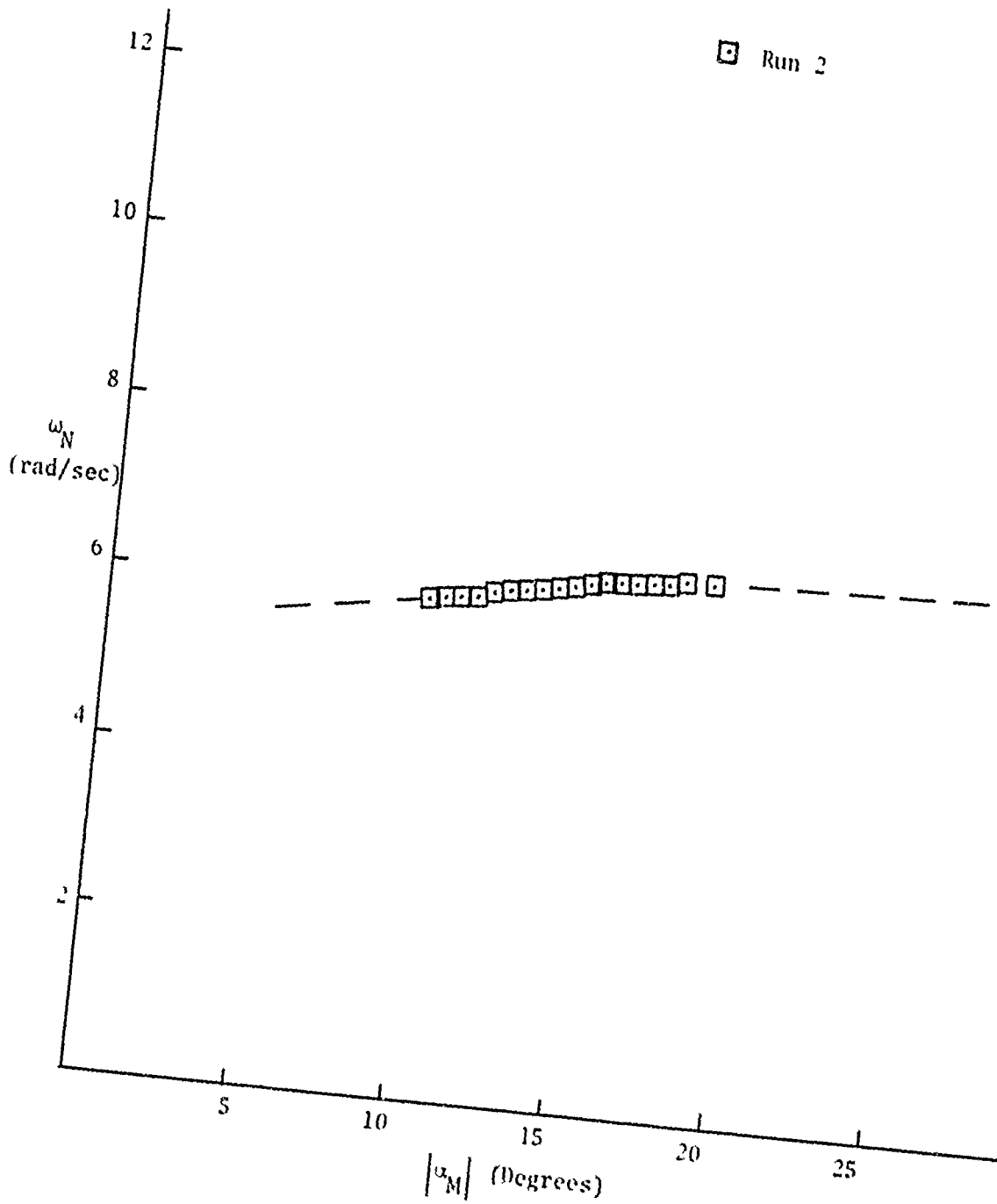


Figure 20 (c). Nutation Frequency for N-Vane 2 Configuration

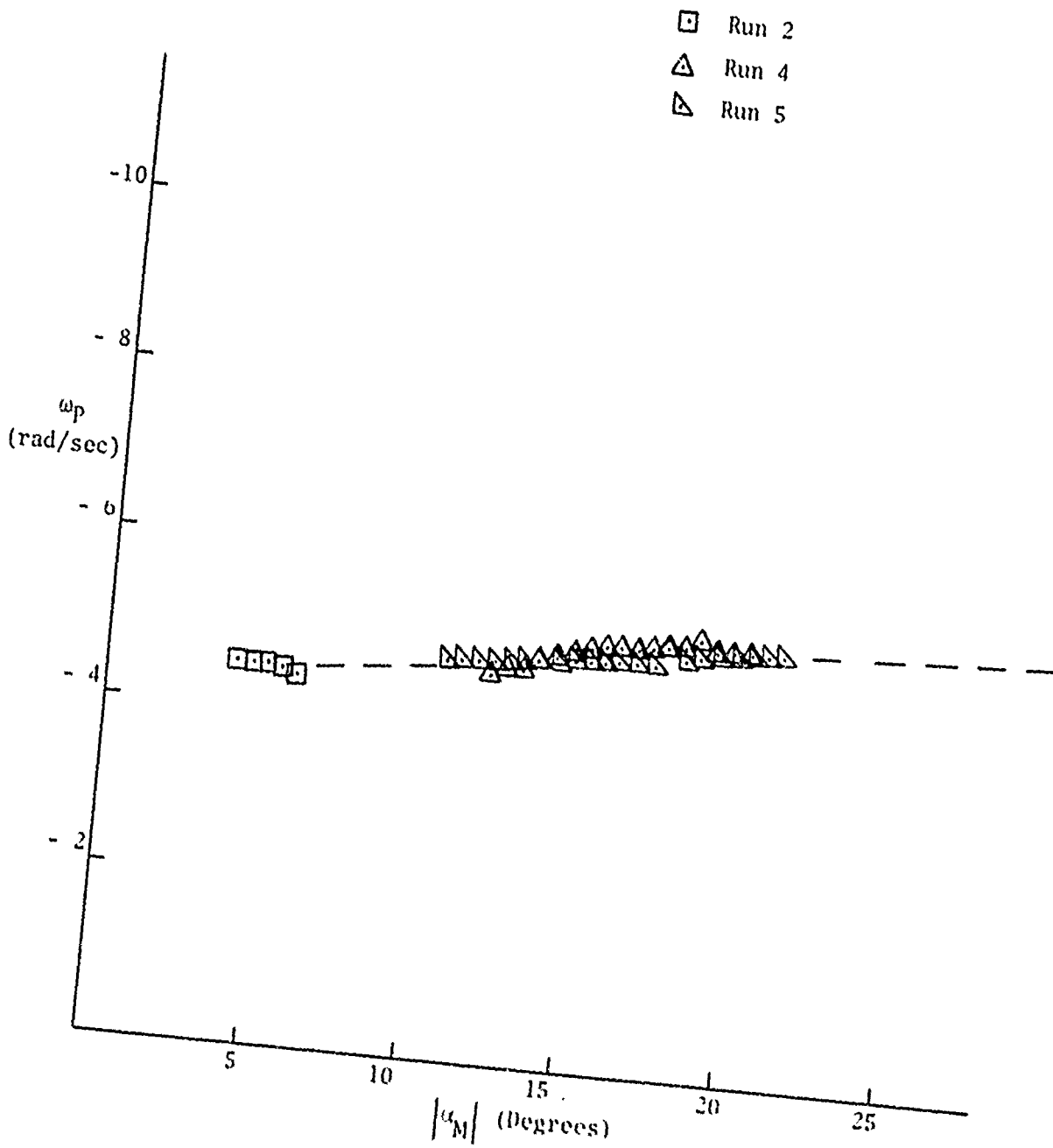


Figure 21 (a). Precession Frequency for Clean Configuration from 3-D Test

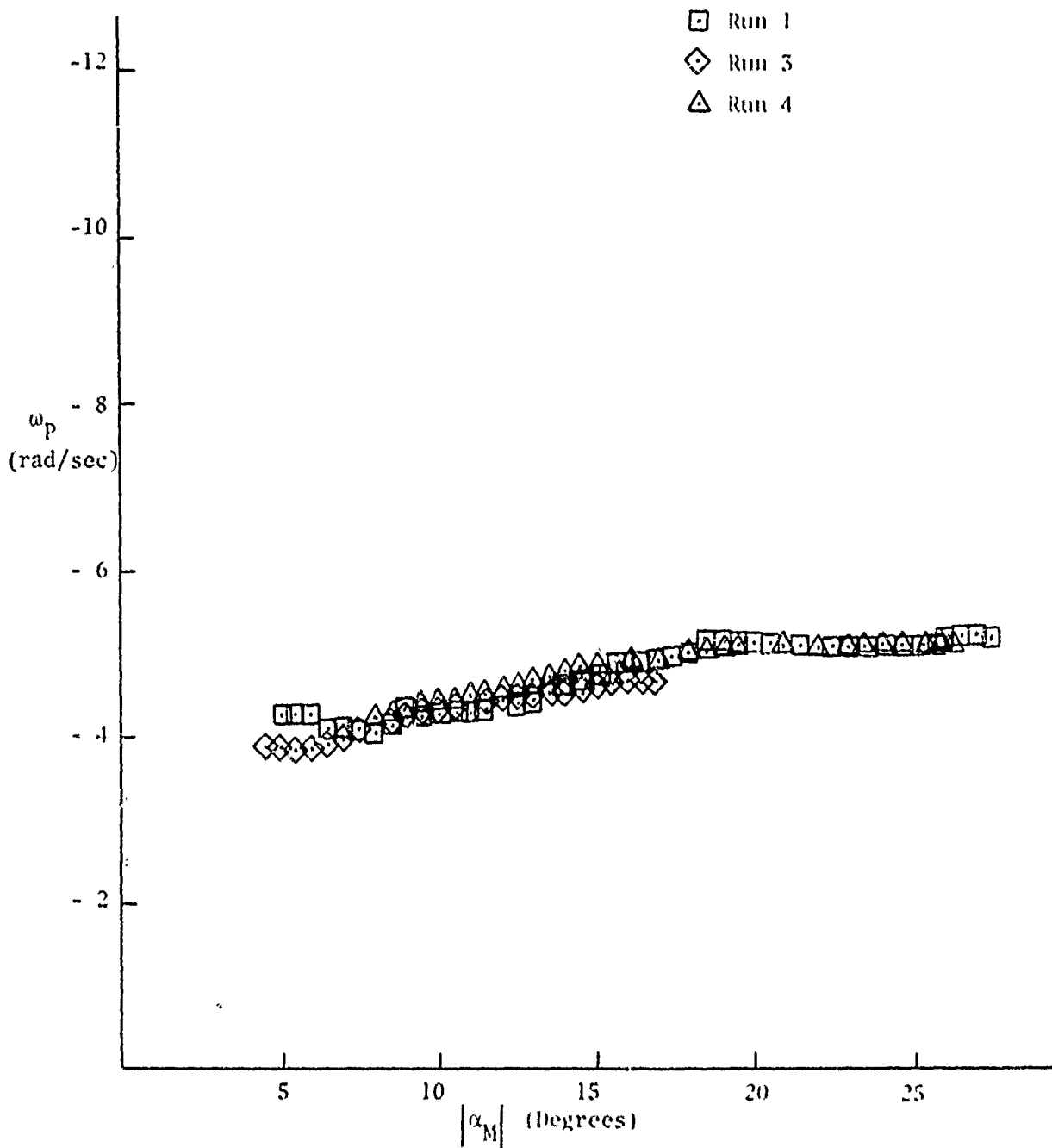


Figure 21 (b). Precession Frequency for N-Vane 1 Configuration from 3-D Test

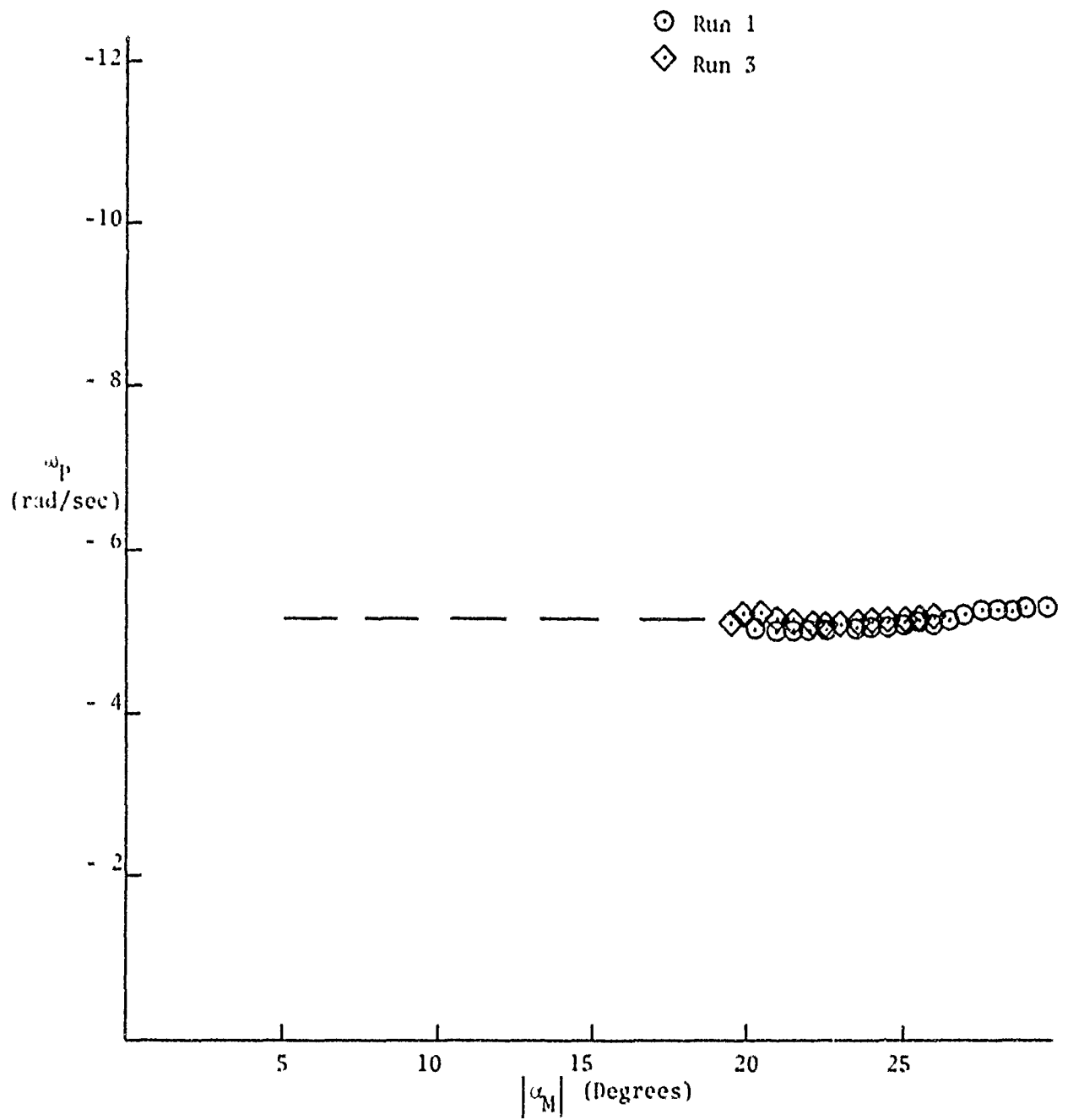


Figure 21 (c). Precession Frequency for N-Vane 2 Configuration

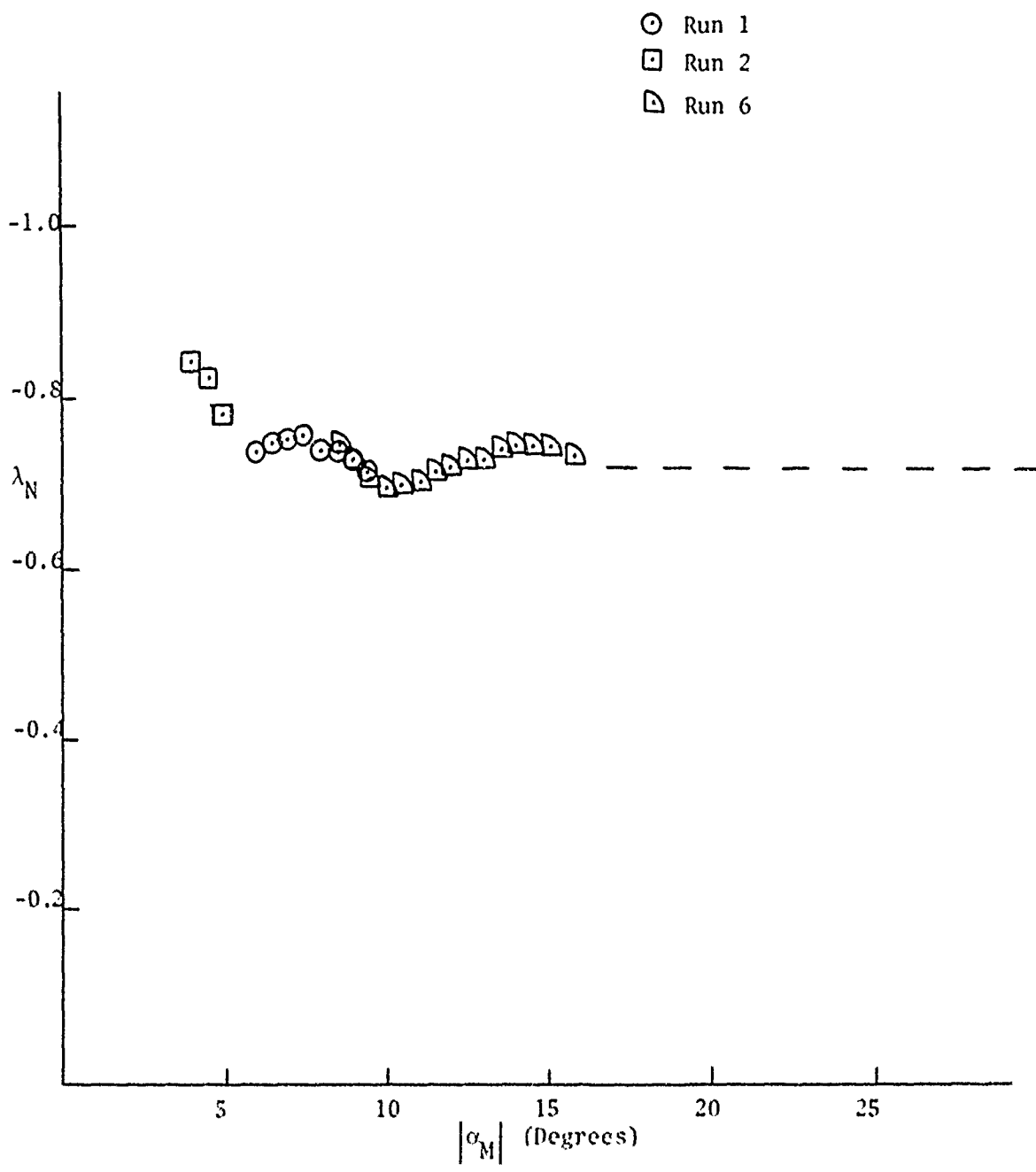


Figure 22 (a). Nutation Dynamic Damping Factor for Clean Configuration from 3-D Test

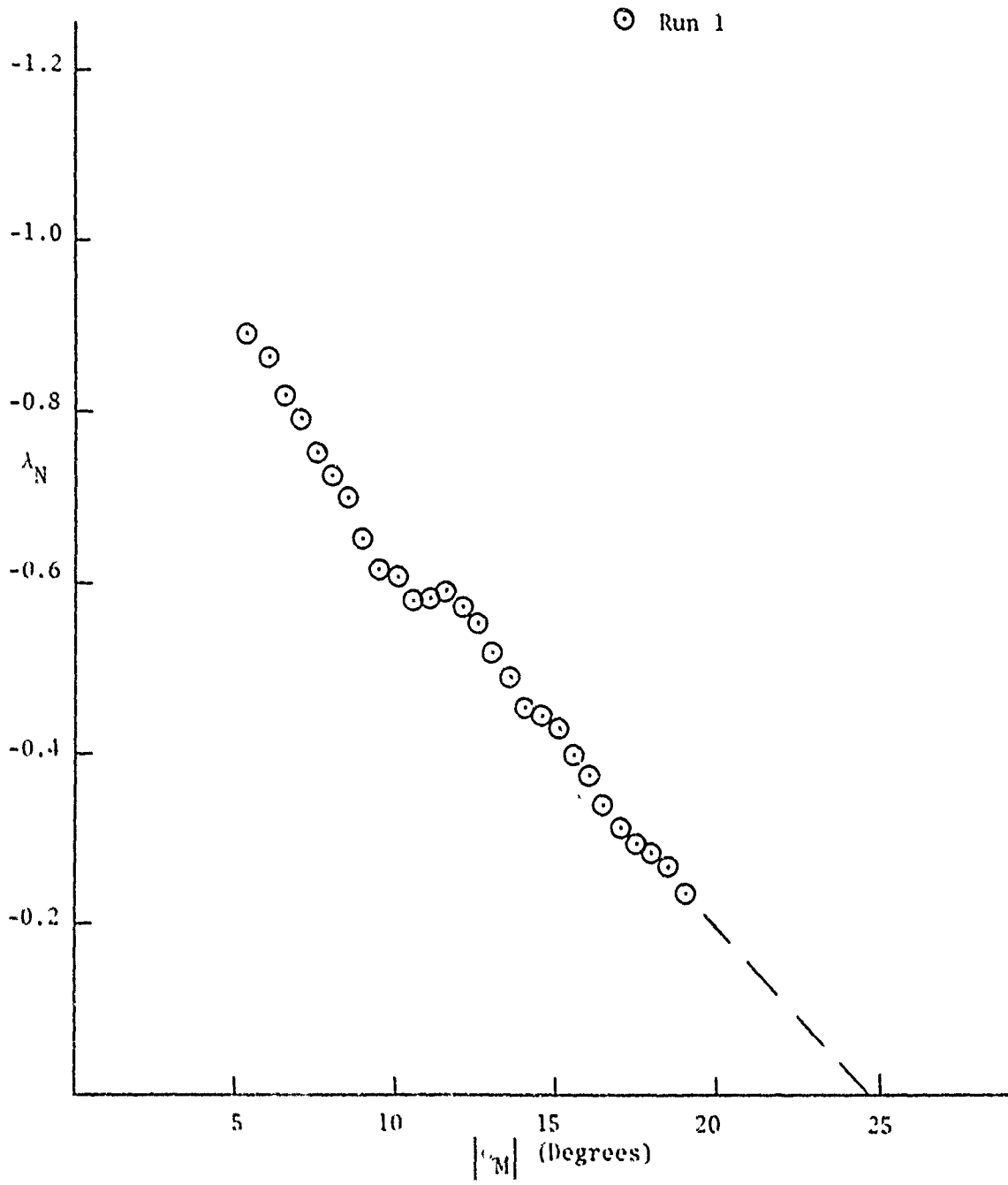


Figure 22 (b). Nutation Dynamic Damping Factor for N-Vane 1 Configuration from 3-D Test

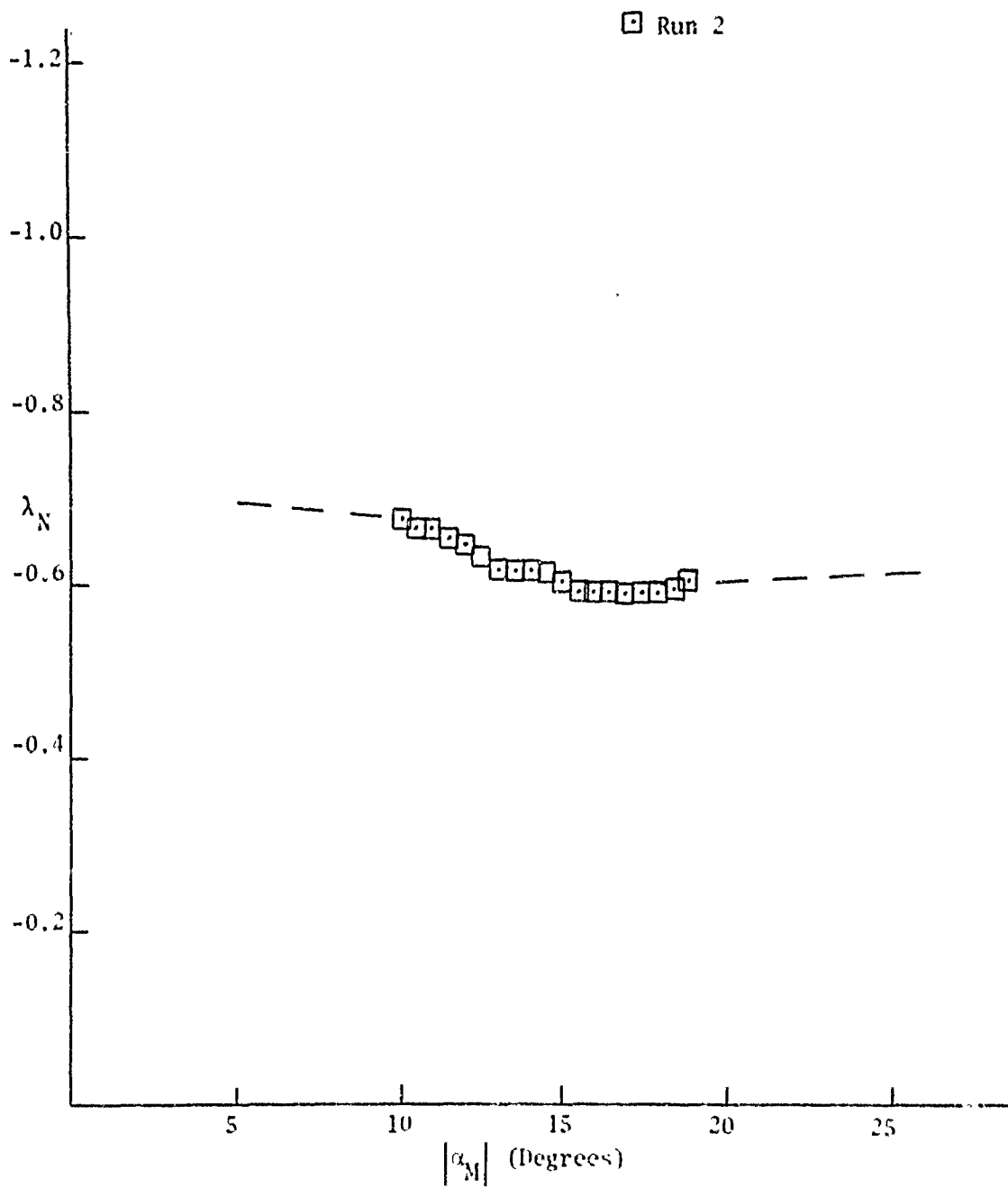


Figure 22 (c). Nutation Dynamic Damping Factor for N-Vane 2 Configuration from 3-D Test

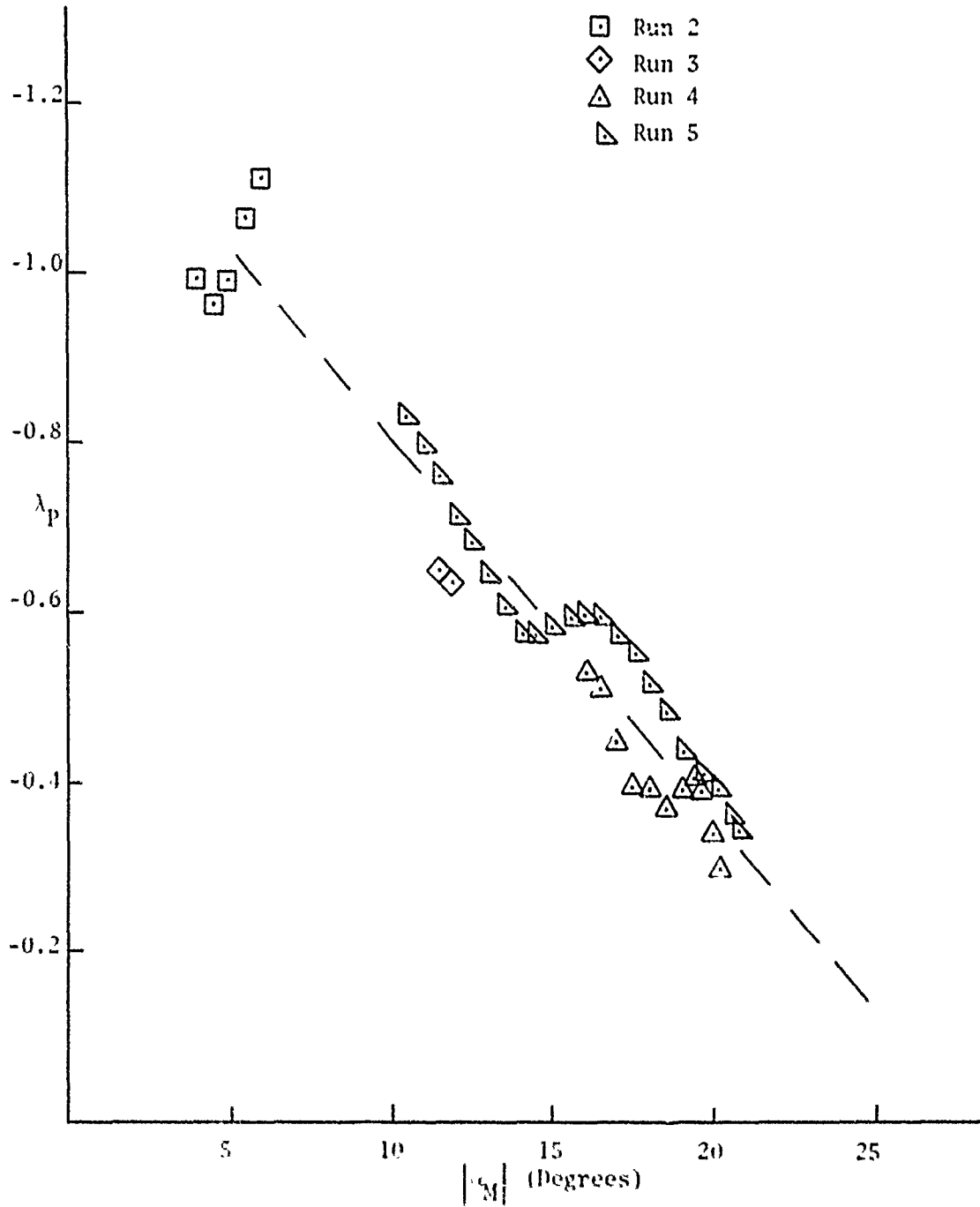


Figure 23 (a). Precession Dynamic Damping Factor for Clean Configuration from 3-D Test

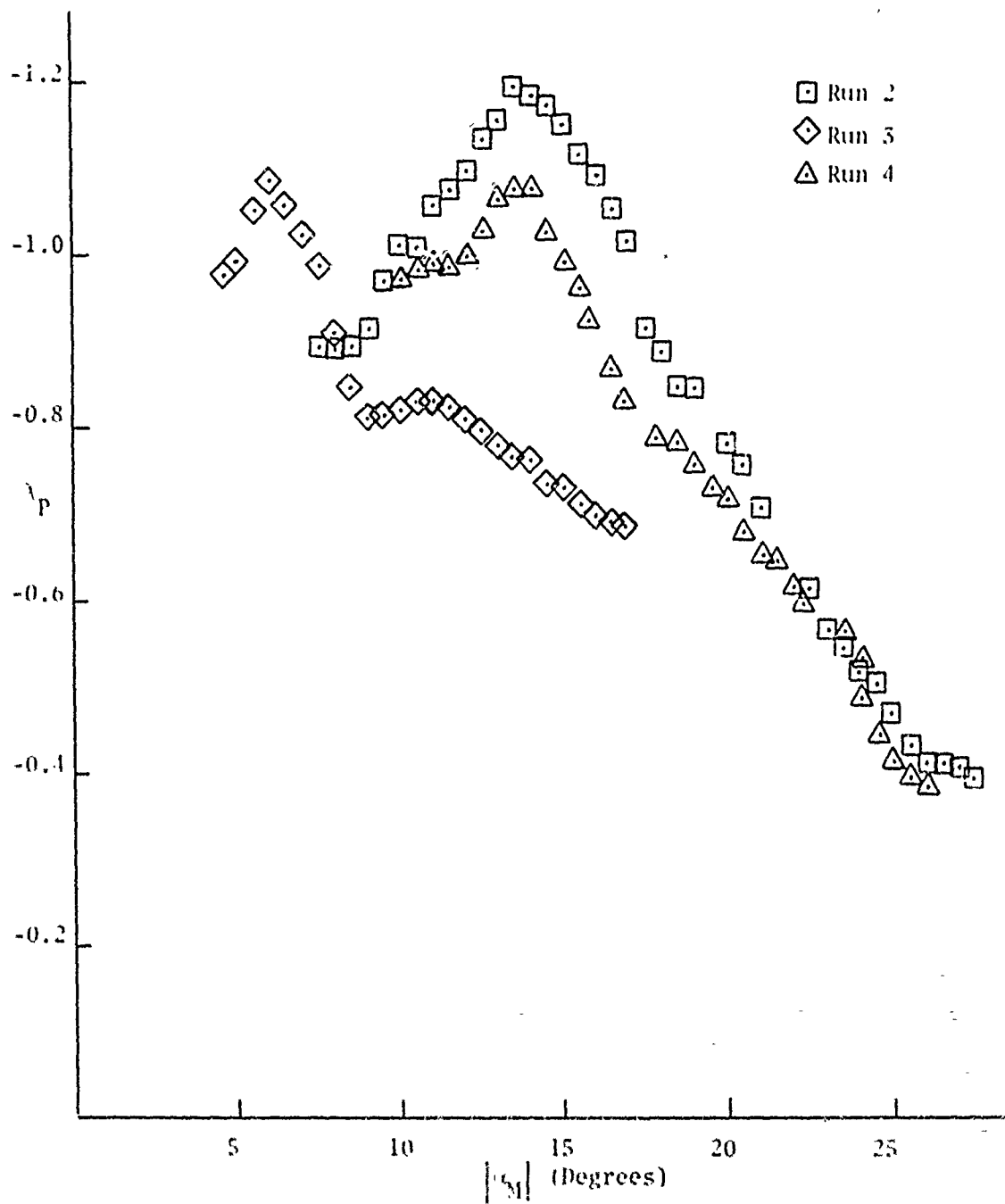


Figure 23 (b). Precession Dynamic Damping Factor for N-Vane 1 Configuration from 3-D Test

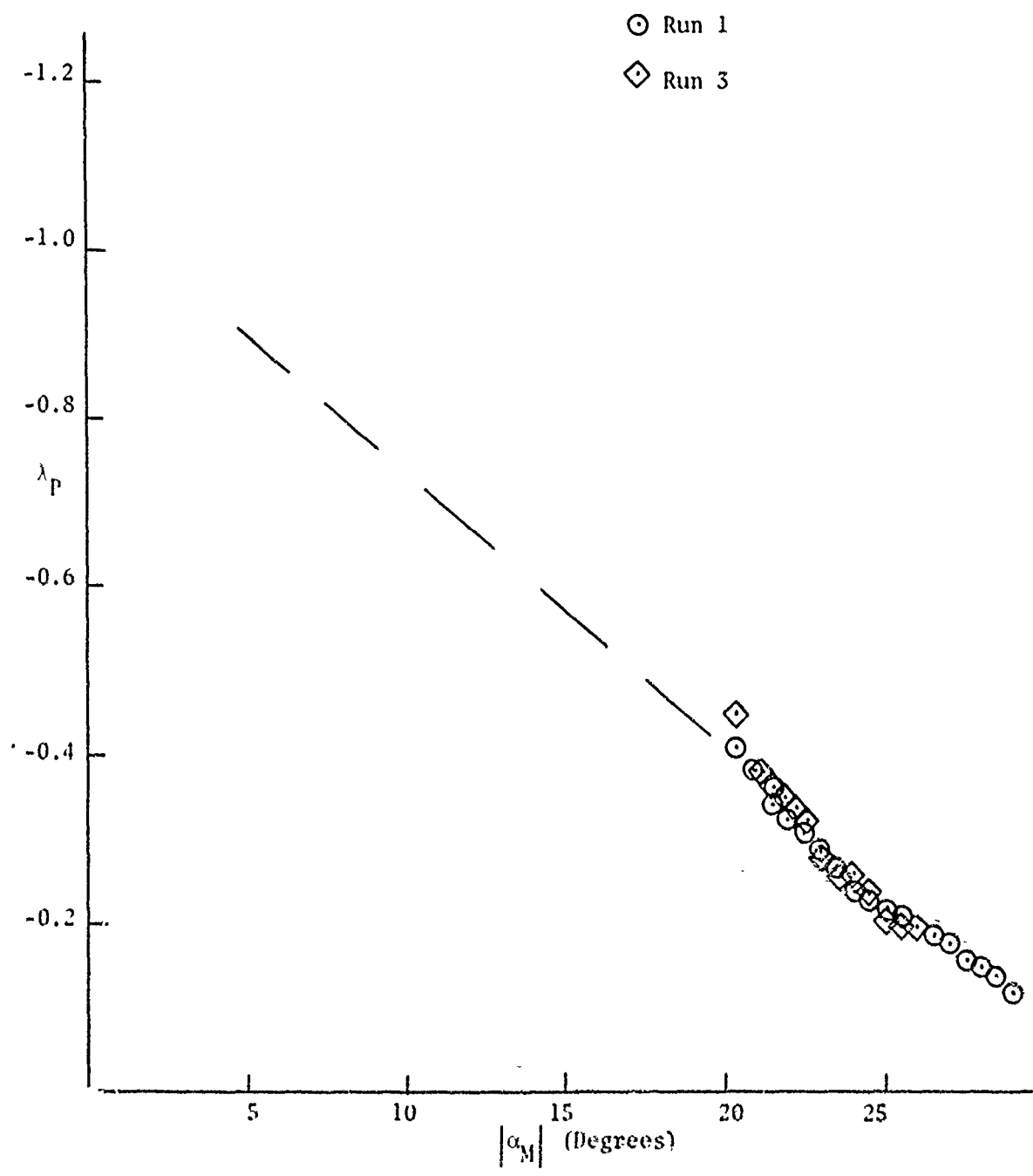


Figure 23 (c). Precession Dynamic Damping Factor for N-Vane 2 Configuration

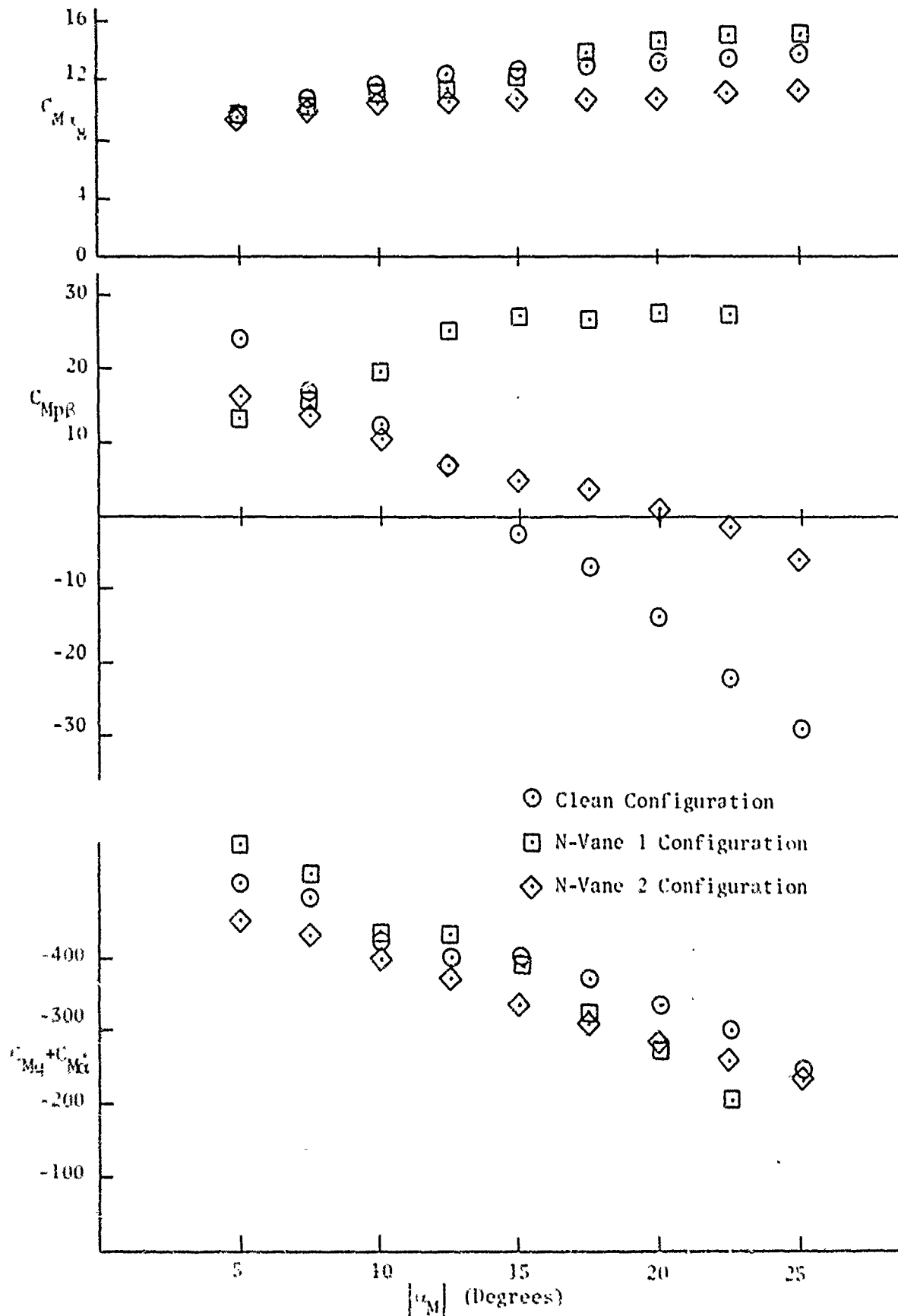


Figure 24. Summary of Aerodynamic Coefficients

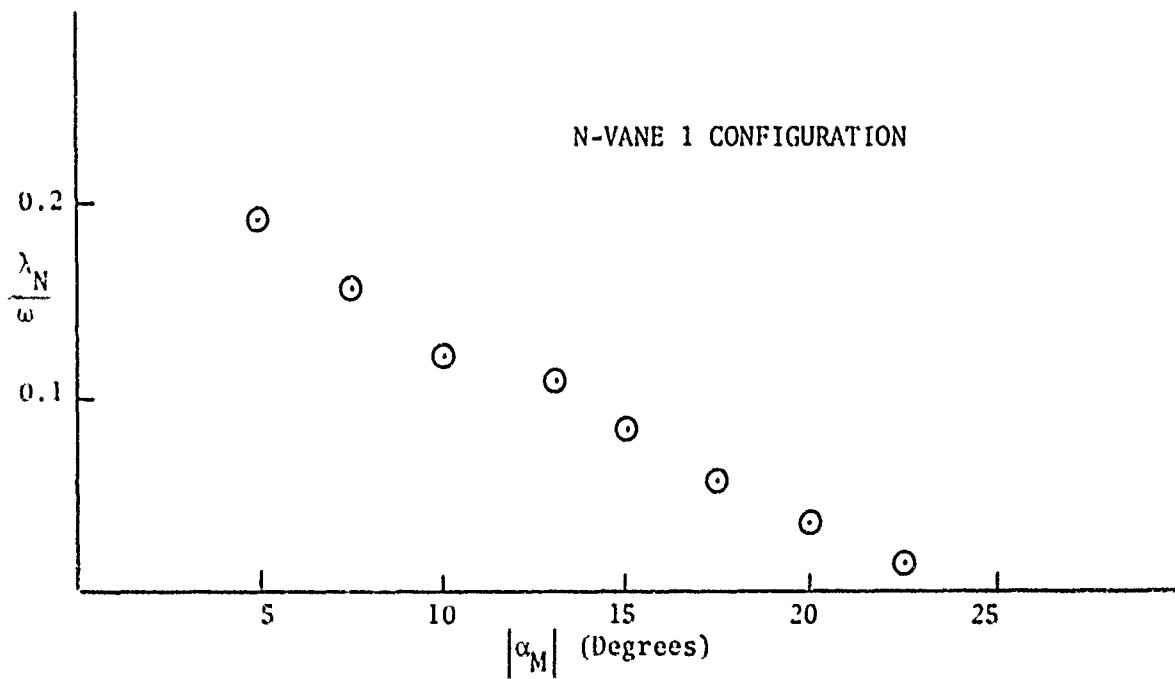
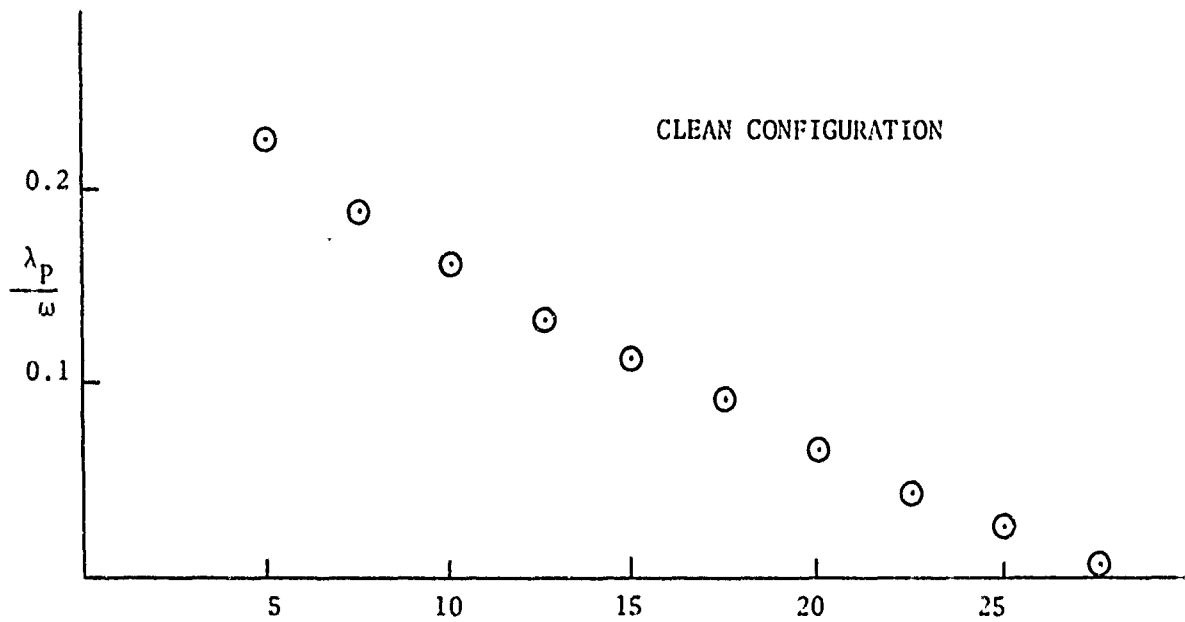


Figure 25. Dynamic Damping Factors for Limit Cycle Motions

TABLE II. SUMMARY OF 3-D WIND TUNNEL TESTS				
CONFIGURATION	α M RANGE, Degrees		ROLL RATE, rad/sec	TYPE OF MOTION
1. Clean	9.5	6.0	57.4	Nutation
2. Clean	6.0	4.0	59.5	Precession
3. Clean	(Unable to obtain a fit)		55.2	Precession
4. Clean	20.2	12.0	56.0	Precession
5. Clean	20.7	10.5	55.5	Precession
6. Clean	15.7	8.5	57.4	Nutation
1. N-Vane 1	19.0	15.3	49.3	Nutation
2. N-Vane 1	27.4	5.0	42.8	Precession
3. N-Vane 1	16.4	4.5	51.8	Precession
4. N-Vane 1	10.0	7.2	44.5	Precession
1. N-Vane 2	29.7	20.3	54.3	Precession
2. N-Vane 2	18.8	10.0	48.7	Nutation
3. N-Vane 2	25.8	19.6	54.7	Precession

TABLE III. SUMMARY OF MOTION HALF-LIVES				
Half-life = $\frac{1}{\lambda_{N,P}}$ ln $\frac{1}{2}$ (Seconds)				
Half-life = $\frac{1}{d\lambda_{N,P}}$ ln $\frac{1}{2}$ (Calibers)				
CONFIGURATION	PRECESSION, Seconds	HALF-LIFE, Calibers	NUTATION, Seconds	HALF-LIFE, Calibers
Clean	-	-	0.94	462.2
N-Vane 1	0.72	360	-	-
N-Vane 2	1.15	570	1.15	590
Note: The values chosen for $\lambda_{N,P}$ were for $ \alpha_M = 15$ degrees				

1. RESULTS FOR CLEAN CONFIGURATION

The pitching moment coefficient ($C_{M\alpha}$) was similar for all the configurations. The pitch damping moment coefficient and Magnus moment coefficient for the clean configuration are plotted in Figures 18(a) and 19(a). The magnitude of $C_{Mq} + C_{M\dot{\alpha}}$ decreases with increasing angle of attack; whereas, $C_{Mp\beta}$ went from a positive value at small angles to a negative value at the large angles. This was expected because a negative $C_{Mp\beta}$ destabilized the precession arm and caused the limit cycle at about 35 degrees. Also λ_p was found to go to zero in this range of angles of attack indicating a limit cycle. The dynamic stability criteria of Equation (15) showed that for values of $s = -0.044$ (from Equation 14) and $\tau = 0.205$ (from Equation 13), and using the coefficients from Figures 18(a) and 19(a), the clean configuration was dynamically unstable for angles larger than approximately 25 degrees.

2. RESULTS FOR N-VANE 1 CONFIGURATION

Pitch damping and Magnus moment data for the N-vane 1 configuration are shown in Figures 18(b) and 19(b). The magnitude of $C_{Mq} + C_{M\dot{\alpha}}$ again decreased with increasing angle of attack. The Magnus moment $C_{Mp\beta}$ did not change sign as it did for the clean configuration, but instead it increased in the positive direction with increasing angle of attack. This again confirmed the observed motions because a positive $C_{Mp\beta}$ destabilized the nutation arm leading to the nutation limit cycle as shown in Figure 6 and in the plot of λ_N in Figure 22(b). Using these values for $C_{Mq} + C_{M\dot{\alpha}}$ and $C_{Mp\beta}$, Equation (15) again showed a dynamic instability at approximately 25 degrees.

3. RESULTS FOR N-VANE 2 CONFIGURATION

Pitch damping and Magnus moment data for the N-vane 2 configuration are plotted in Figures 18(c) and 19(c). The pitch damping moment coefficient had the same trend as for the previous two cases. The Magnus moment coefficient was positive at small angles and changed sign at the higher angles. This was the same trend as was obtained for the clean configuration; however, the magnitude of $C_{Mp\beta}$ was less at both the low and high angles than it was for the clean configuration. These values of $C_{Mq} + C_{M\dot{\alpha}}$ and $C_{Mp\beta}$ used in the dynamic stability criteria equation showed that this configuration was dynamically stable at all angles over which it was tested. This confirmed the observed motion, as no limit cycles or instabilities were observed for this configuration.

4. RESULTS OF FLOW VISUALIZATION TESTS

The smoke flow pictures taken for the three configurations are shown in Figures 26 and 27. The flow over the clean configuration at zero spin rate was laminar. At the terminal spin rate, the flow over the clean configuration was slightly turbulent. The N-vane 1 configuration caused the boundary layer to become more turbulent and to increase in thickness. The N-vane 2 configuration increased the boundary layer turbulence and thickness more than the clean configurations, although not nearly as much as for the N-vane 1 configuration.

5. RESULTS IN NONLINEAR DATA REDUCTION

Since motions containing limit cycles are obviously nonlinear, a nonlinear data reduction procedure as described in References 2 and 5 was used to compute nonlinear coefficients for all the configurations. Due to the one-armed nature of the motions, most of the coefficients obtained contained a large amount of scatter and therefore are not presented.



(a) Zero Spin Rate



(b) Steady State Spin Rate

Figure 26. Smoke Flow over Clean Configuration



(a) N-Vane 1 Configuration



(b) N-Vane 2 Configuration

Figure 27. Smoke Flow Over N-Vane Configurations at Steady Spin Rate

SECTION VI

CONCLUSIONS AND RECOMMENDATIONS

The effect of N-vanes on the 3-D angular motion of a rolling finned missile has been analyzed. The aerodynamic coefficients $C_{M\dot{\alpha}}$, $(C_{M\dot{\alpha}} + C_{M\ddot{\alpha}})$, and $C_{M\dot{\beta}}$ were obtained for a clean configuration and for two turning vane configurations.

The clean configuration had a precession limit cycle of about 35 degrees amplitude caused by the Magnus moment having a large negative value in this region of angles of attack.

The effect of the N-vanes 1 configuration was to eliminate the precession limit cycle by preventing the Magnus moment from becoming large negatively with increasing angle of attack. The nutation limit cycle of about 25 degrees obtained for this configuration was caused by the large positive value for the Magnus moment in the 25 degree angle of attack region.

The N-vane 2 configuration eliminated both the precession and nutation limit cycles by keeping the magnitude of the Magnus moment small for the entire angle of attack range.

N-vanes added to the nose of a rolling finned missile were effective in altering the Magnus characteristics and hence the dynamic stability of the missile.

Since most finned missiles encounter a wide range of Reynolds numbers, Mach numbers, and roll rates over their flight regime, additional experimental and analytical work is required to determine if N-vanes can be effective for eliminating Magnus instabilities in the actual use of the missile.

Wind tunnel testing should be conducted at higher velocities over a range of spin rates and angles of attack. If the results are promising, full scale free flight tests should be performed.

REFERENCES

1. Nicolaides, J. D.: Free Flight Missile Dynamics, Aero-Space Engineering Dept., University of Notre Dame, 1961.
2. Ingram, C. W.; Butler, C. B.; Martin, J.; and Vasquez, R.: A Three-Degrees-of-Freedom Wind Tunnel Testing Procedure. AFATL-TR-67-195, Volume I, Air Force Armament Laboratory, October 1967.
3. Butler, Carroll B.: 2.75-Inch FFAR Large Yaw Dynamics. AFATL-TR-68-43, Air Force Armament Laboratory, March 1968.
4. Eikenberry, R. S.: Analysis of the Angular Motion of Missiles. Department of Aero-Space Engineering, University of Notre Dame, SC-CR-70-6051, February 1970.
5. Murphy, C. H.: Free Flight Motion of Symmetric Missiles. Ballistic Research Laboratories Report No. 1216, Ballistic Research Laboratories, July 1963.
6. Brown, F. N. M.: See The Wind Blow. Department of Aerospace and Mechanical Engineering, University of Notre Dame. 1971.
7. Nicolaides, J. D.; Ingram, C. W.; Martin, J.; Morrison, A.: Nonlinear Aerodynamic Characteristics of the 2.75 Wrap-Around Fin Configuration, presented at 8th Navy Symposium on Aeroballistics, Naval Weapons Center, China Lake, California, May 1969.
8. Nicolaides, J. D.: A History of Ordnance Flight Dynamics. American Institute of Aeronautics and Astronautics Paper No. 70-533, May 1970.